

UCSF

UC San Francisco Electronic Theses and Dissertations

Title

Development of Inhibitors for Phosphatidylinositol Kinases

Permalink

<https://escholarship.org/uc/item/11h8c4n8>

Author

Tavshanjian, Brandon Harold

Publication Date

2011

Peer reviewed|Thesis/dissertation

Development of Inhibitors for Phosphatidylinositol Kinases

by

Brandon Harold Tavshanjian

DISSERTATION

Submitted in partial satisfaction of the requirements for the degree of

DOCTOR OF PHILOSOPHY

in

Chemistry and Chemical Biology

in the

GRADUATE DIVISION

of the

UNIVERSITY OF CALIFORNIA, SAN FRANCISCO

Copyright 2010

by

Brandon Harold Tavshanjian

DEVELOPMENT OF INHIBITORS FOR PHOSPHATIDYLINOSITOL KINASES

Brandon Harold Tavshanjian

The development of small-molecule inhibitors for two types of human phosphatidylinositol kinases (class III PI3-kinase and class III PI4-kinase) is described. The first part consists of an analysis of structural differences between class I PI3-kinase and class III PI3-kinase, followed by structure-guided synthesis of inhibitors exhibiting moderate specificity for class III PI3-kinase over class I PI3-kinase. The second part consists of combinatorial synthesis and assay-guided development of inhibitors for class III PI4-kinase alpha and beta, with the goal of producing compounds useful for the inhibition of HCV genotype 2a replication in hepatocytes with minimal toxicity. Several examples of compounds exhibiting varying selectivity for class III PI4-kinase over the evolutionarily related class I PI3-kinases and protein kinases are ultimately developed, including compounds which are effective at inhibiting HCV replication in hepatocytes at sub-micromolar concentrations.

TABLE OF CONTENTS

LIST OF TABLES	v
LIST OF FIGURES	vi
INTRODUCTION	1
References.....	7
CHAPTER 1: STRUCTURAL FEATURES OF INHIBITORS OF VPS34.....	9
Experimental Methods.....	22
References.....	37
CHAPTER 2: DEVELOPMENT OF PHENYLTHIAZOLE INHIBITORS FOR PHOSPHATIDYLINOSITOL 4-KINASES.....	39
Experimental Methods.....	55
References.....	72
CHAPTER 3: NEW SIGNALING ROLES FOR HUMAN CARBONYL REDUCTASE I REVEALED BY ENZYMOLOGY.....	74
Experimental Methods.....	86
References.....	89

LIST OF TABLES

Table	Page
Table 1: Features of PIK Kinases	3

LIST OF FIGURES

Figure	Page
INTRODUCTION	
Figure 1: Cellular abundance of phosphoinositide species	4
Figure 2: Domain architecture of related mammalian PIK kinases.	5
Figure 3: Protein alignment of human PIK kinase domains from class I PI3K (p110 α , p110 β , p110 γ , p110 δ), class II PI3K (PI3KC2 α , PI3KC2 β , PI3KC2 γ), class III PI3K (Vps34), and class III PI4K (PI4KIII α and PI4KIII β).	6
CHAPTER 1: STRUCTURAL FEATURES OF INHIBITORS OF VPS34	
Figure 1: Features of PI3-kinases.	11
Figure 2: Comparison of binding mode of PIK-93 to DmVps34 (pdb code 2X6J) and Hsp110g (pdb code 2CHZ).	13
Figure 3: 3-methyladenine binding to Vps34.	15
Figure 4: Structural differences between PIK93-Dmvps34 (pdb code 2X6J) and PIK93-Hsp110g (pdb code 2CHZ).	18
Figure 5: Synthesis of PIK93 analogs.	20

CHAPTER 2: DEVELOPMENT OF PHENYLTHIAZOLE INHIBITORS FOR PHOSPHATIDYLINOSITOL 4-KINASES

Figure 1: Inhibition of p110a, p110g, PI4KIIIa and PI4KIIIb by 5-phenylthiazole panel.	42
Figure 2: Cellular activity of selected phenylthiazole inhibitors in an HCV genotype 2a system.....	43
Figure 3: Summary of single-point inhibition of protein kinases by PIK93 and PT19..	46
Figure 4: Change in inhibition of protein kinases by PIK93 and PT19.....	47
Figure 5: Effect of sulfonamide alkyl substitution on lipid kinase inhibition.....	49
Figure 6: Effect of N-phenylsulfonamide derivatization on lipid kinase inhibition..	51
Figure 7: Further derivatization of N-phenylsulfonamide inhibitors.....	52
Figure 8: Summary of inhibitor development and SAR relationships gleaned from this survey.....	53

CHAPTER 3: NEW SIGNALING ROLES FOR HUMAN CARBONYL REDUCTASE I REVEALED BY ENZYMOLOGY

Figure 1: Fold and structural features of CBR1-OH-PP-NADP (PDB code 1WMA).....	75
Figure 2: Diversity and function of CBR1 reduction.....	76
Figure 3: Kinetic data for CBR1 reduction.....	79
Figure 4: In vitro analysis of GSNO reduction.....	81

Figure 5: Structural comparison of hCBR1 (pdb 3BHJ) and hCBR3 (pdb 2HRB).....84

INTRODUCTION

Due to the substantial biosynthetic complexity of eukaryotic cells and their intensive requirement for compartmentalization, the cellular membranes of eukaryotes contain a large array of phospholipids with diverse physical properties. From zwitterionic phospholipids such as phosphatidylethanolamine and phosphatidylcholine, to anionic phospholipids like phosphatidylserine and phosphatidylinositol, at least nine different entities comprise the membrane complement of phospholipids¹. These phospholipids can be employed for either structural or signaling roles. On one hand, the relative content of individual phospholipids can modulate bilayer architecture, having effects on membrane fusion or integration of protein components into the membrane; on the other hand, enzymatic modification of phospholipids in the membrane can serve to produce chemical second messengers to mediate intracellular processes. Some phospholipids seem to play a primarily structural role and have very long half lives in cells: an example is cardiolipin (CL), which has been observed to form non-bilayer structures under physiological conditions suggested to play a role in protein translocation into mitochondria² and having a half-life of days³. However, other phospholipids may play a more central capacity, being involved in both structural and signaling roles and having an intermediate rate of turnover: the best example of this class is phosphatidylinositol (PI). This is no arbitrary coincidence; whereas other lipids possess only a single derivatizable handle (i.e. the amine of phosphatidylethanolamine), phosphatidylinositol possesses five hydroxyls capable of modification—and it is the ability of eukaryotic phosphatidylinositol kinases to modify PI into a diverse array of phosphatidylinositol phosphates (PIPs, Figure 1) that allows PI to play a central role in cellular function.

Phosphatidylinositol Phosphates

The structure/signaling divide in functions of PIP species parallels the divide in functions of phosphoinositides; while all play some role in cellular signaling, PIPs vary dramatically in half-life and abundance and thus some play roles more related to transient pulse signaling while others are involved in dynamic but constitutive cellular processes. For example, PI(3,4,5)P₃, which has probably the lowest abundance in eukaryotic cells (~0.03%⁴) and the shortest half life (<1 min⁵), is probably the best-known signaling phospholipid, playing a central role in cellular responses to insulin and growth factors⁶. In contrast, PI(3)P, which mediates trafficking of endosomal cargo to lysosomes⁷ and PI(4)P, which mediates post-Golgi cargo transport⁸, have higher abundances (figure 1) and longer-half lives (~8 min⁹ and 2-5 hours¹⁰).

Phosphatidylinositol Kinases

Just as the abundance and half-life of phosphoinositides suits their intracellular roles, so too is the architecture of the phosphatidylinositol kinases which produce them are optimized for the purpose in which these kinases are employed within the cell. In eukaryotes, all PI3- and the class III PI4- kinases are evolutionarily related, sharing a common lipid kinase domain preceded by a helical domain unique to their class that likely derives from ancestral Vps34, the oldest PIK. In addition to a frequently observed C2 domain that likely plays a role in recruiting the kinases to their substrate phosphoinositides¹¹, PIKs also possess various domain modules that facilitate interactions with their regulatory partners (Figure 2, Table 1). In the case of class I PI3K which require rapid and transient activation by receptors, the enzymes exist as

heterodimers with receptor-responsive regulatory subunits (p85/p55/p101) in addition to possessing domains that allow activation by the G-protein Ras. In the case of other PIKs which have more of a constitutive signaling role such exquisite regulation is absent (class III PI3K, class III PI4K), and the enzymes comprise simpler structures occasionally interrupted by binding elements.

Table 1: Features of PIK Kinases

Enzyme	Substrate	Regulatory Subunit	Localization	Activators
Class I PI3K p110 $\alpha/\beta/\delta$ p110 γ	PtdIns(4,5)P ₂	p85 α /p85 β /p55 γ p101 (p110g)	Plasma Membrane	Ras, RTK ¹²
Class III PI3K Vps34	PtdIns	p150	Early Endosomes ¹³	Galpha subunits ¹⁴
Class II PI3K PI3KC2 $\alpha/\beta/\gamma$	PtdIns, PtdIns(4)P	None	TGN ¹⁵	RTK
Class III PI4Kα	PtdIns	None	Nucleus/ER	Arf1 ⁸
Class III PI4Kβ	PtdIns	None	Golgi	Arf1 ⁸

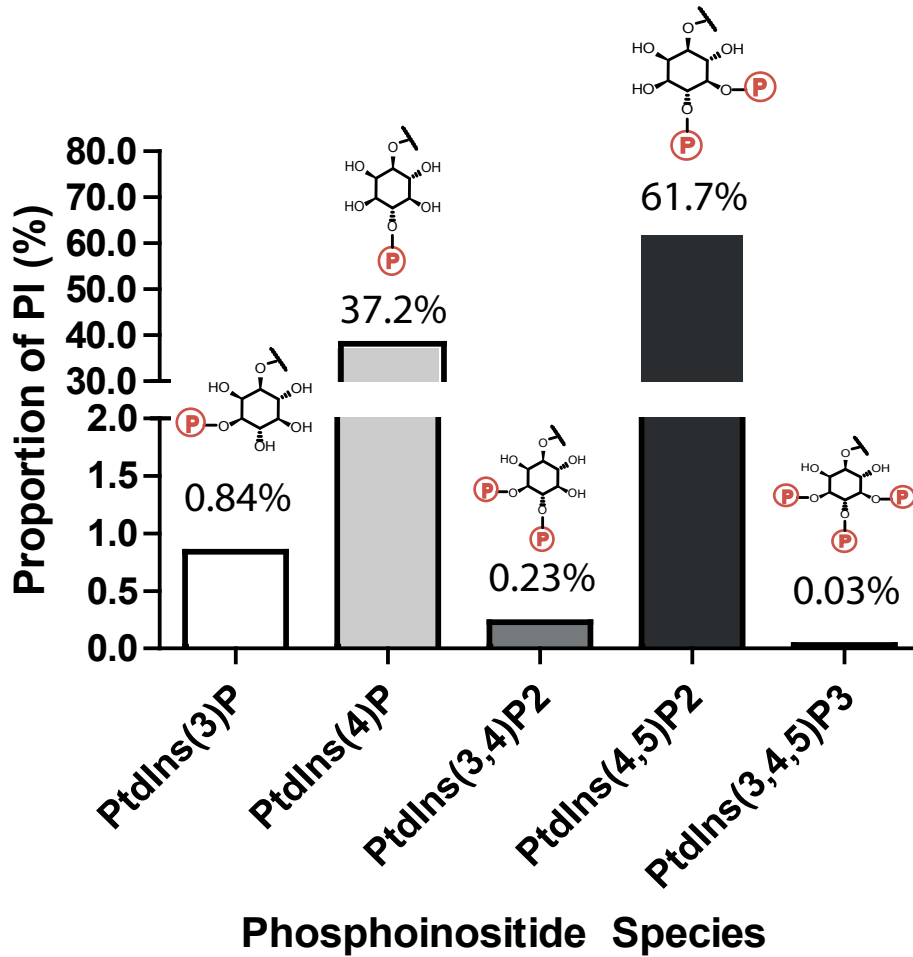


FIGURE 1: Cellular abundance of phosphoinositide species. Representative levels of phosphoinositide species in unstimulated cells (derived from Guillou et al. Methods Enzymol. 2007;434:117-30.)

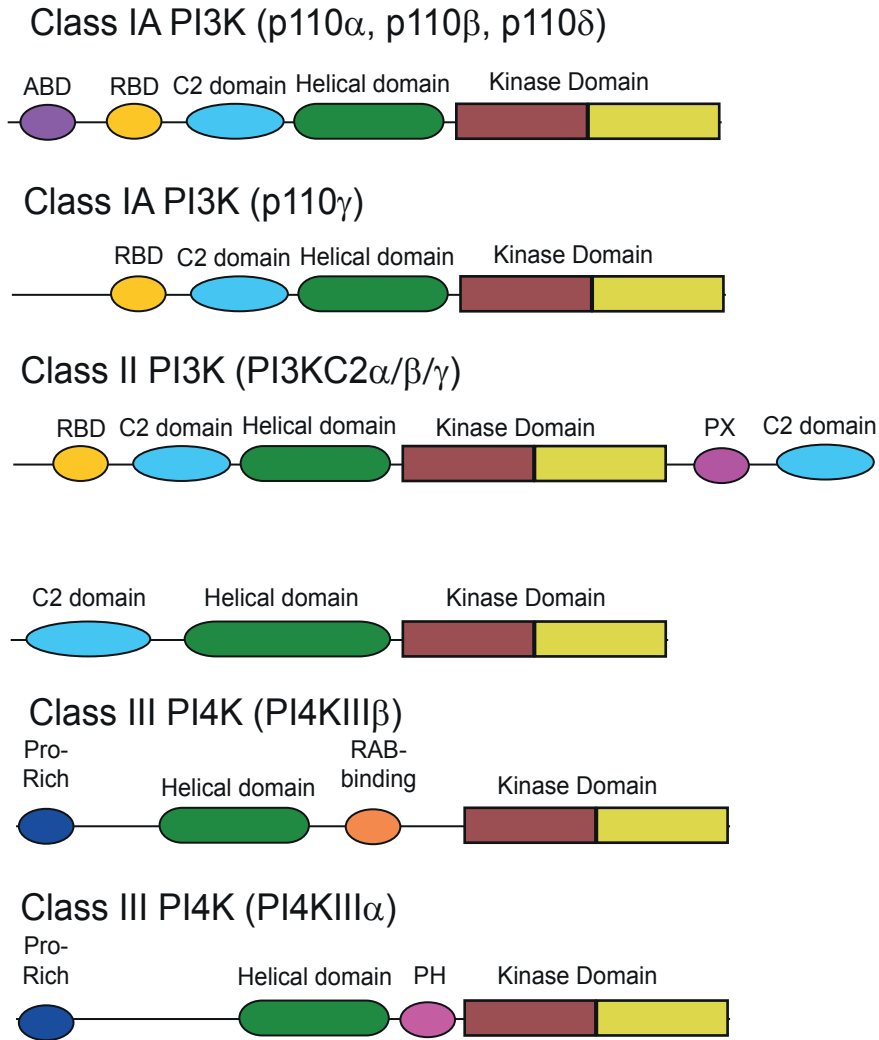


FIGURE 2: Domain architecture of related mammalian PIK kinases. The evolutionarily related class I-III PI3K and class III PI4K share a common lipid kinase-helical domain core supplemented by accessory domains to enhance binding to phospholipids (C2 domain, PH domain, PX domain) and activator/regulatory protein interaction domains (RAB-binding, RBD, ABD).

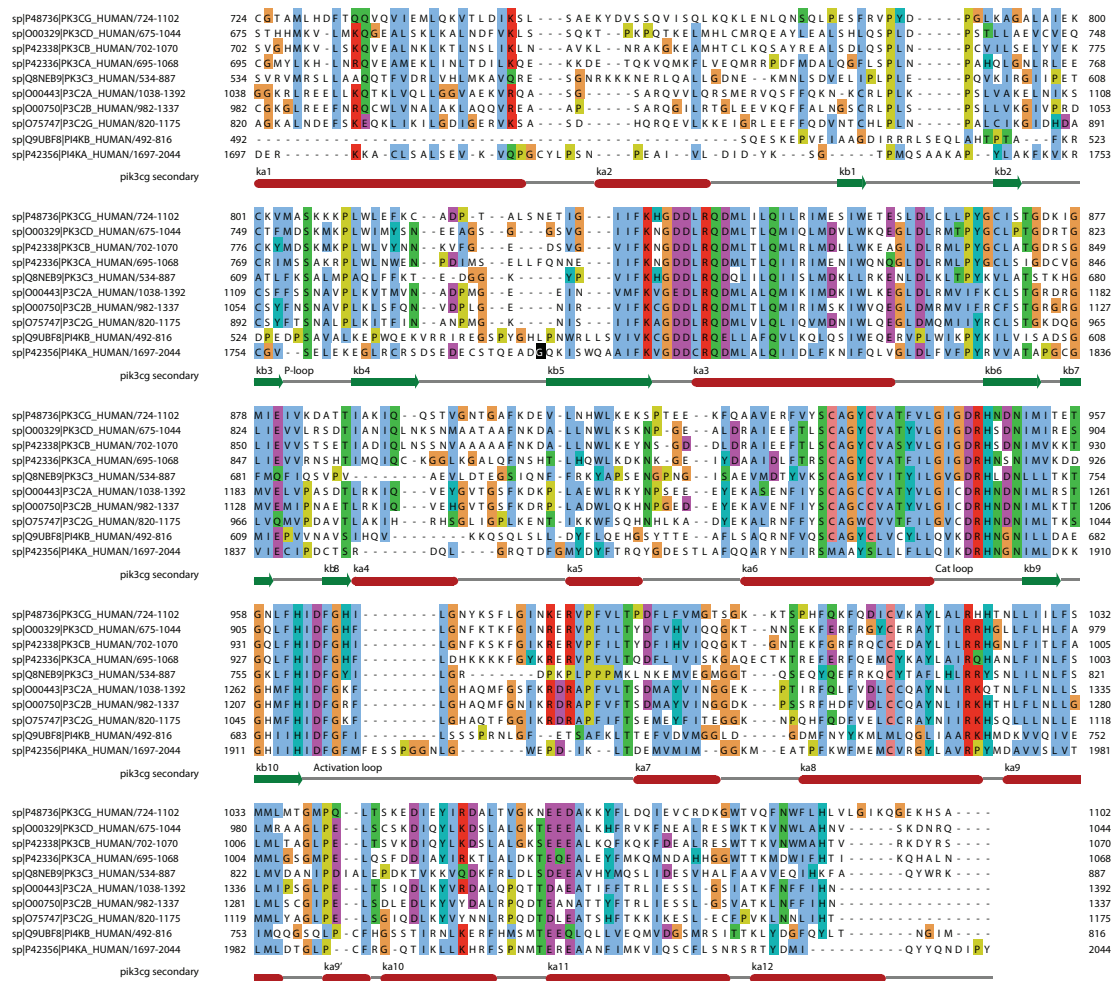


FIGURE 3. Structural Alignment of PIK Kinases. Alignment was generated in SALIGN (Hannes Braberg, Mallur S. Madhusudhan, Ursula Pieper, Ben Webb, Andrej Sali. SALIGN : A multiple protein structure/sequence alignment web server. In preparation. <http://modbase.compbio.ucsf.edu/salign-cgi//index.cgi>). Existing PDB PI3K structures (1E8X, 2X6H, 2RD0, 2WXR) were aligned and used as a template to align human PIK3CA, PIK3CB, PIK3CD, and PIK3CG. The human class II PI3K and class III PI4K were then consecutively added to the alignment.

References

1. Virtanen, J. a, Cheng, K.H. & Somerharju, P. Phospholipid composition of the mammalian red cell membrane can be rationalized by a superlattice model. *Proceedings of the National Academy of Sciences of the United States of America* **95**, 4964-9(1998).
2. Dowhan, W. Molecular basis for membrane phospholipid diversity: why are there so many lipids? *Annual review of biochemistry* **66**, 199-232(1997).
3. Gross, N.J., Getz, G.S. & Rabinowitz, M. Apparent turnover of mitochondrial deoxyribonucleic acid and mitochondrial phospholipids in the tissues of the rat. *The Journal of biological chemistry* **244**, 1552-62(1969).
4. Guillou, H., Stephens, L.R. & Hawkins, P.T. Quantitative measurement of phosphatidylinositol 3,4,5-trisphosphate. *Methods in enzymology* **434**, 117-30(2007).
5. Tengholm, A. & Meyer, T. A PI3-kinase signaling code for insulin-triggered insertion of glucose transporters into the plasma membrane. *Current biology : CB* **12**, 1871-6(2002).
6. Knight, Z.A. et al. A pharmacological map of the PI3-K family defines a role for p110alpha in insulin signaling. *Cell* **125**, 733-47(2006).
7. Schu, P.V. et al. Phosphatidylinositol 3-kinase encoded by yeast VPS34 gene essential for protein sorting. *Science (New York, N. Y.)* **260**, 88-91(1993).
8. Balla, A. & Balla, T. Phosphatidylinositol 4-kinases: old enzymes with emerging functions. *Trends in cell biology* **16**, 351-61(2006).
9. Wurmser, a E. & Emr, S.D. Phosphoinositide signaling and turnover: PtdIns(3)P, a regulator of membrane traffic, is transported to the vacuole and degraded by a process that requires luminal vacuolar hydrolase activities. *The EMBO journal* **17**, 4930-42(1998).
10. Brearley, C.A. & Hanke, D.E. Evidence for substrate-cycling of 3-, 3,4-, 4-, and 4,5-phosphorylated phosphatidylinositols in plants. *The Biochemical journal* **311** (Pt 3, 1001-7(1995).
11. Rizo, J. C2-domains, Structure and Function of a Universal Ca²⁺-binding Domain. *Journal of Biological Chemistry* **273**, 15879-15882(1998).

12. Engelman, J.A., Luo, J. & Cantley, L.C. The evolution of phosphatidylinositol 3-kinases as regulators of growth and metabolism. *Nature reviews. Genetics* **7**, 606-19(2006).
13. Gillooly, D.J. et al. Localization of phosphatidylinositol 3-phosphate in yeast and mammalian cells. *The EMBO journal* **19**, 4577-88(2000).
14. Slessareva, J.E. et al. Activation of the phosphatidylinositol 3-kinase Vps34 by a G protein alpha subunit at the endosome. *Cell* **126**, 191-203(2006).
15. Domin, J. et al. The class II phosphoinositide 3-kinase PI3K-C2alpha is concentrated in the trans-Golgi network and present in clathrin-coated vesicles. *The Journal of biological chemistry* **275**, 11943-50(2000).

CHAPTER 1: STRUCTURAL FEATURES OF INHIBITORS OF VPS34

Classes of PI3-kinases

Phosphatidylinositol 3-kinases, which phosphorylate the D-3 position of membrane-bound phosphatidylinositol, are known to play a role in a diverse array of cellular processes, generating structurally distinct PIPs that serve as binding sites to trigger and organize intracellular events. Three classes of PI3-kinases comprise the complement observed in mammalian cells—the class I PI3-kinases, which phosphorylate PI 4,5-bisphosphate; the class II PI3-kinases, which are capable of phosphorylating PI 4,5-bisphosphate and PI 4-phosphate; and the class III PI3-kinases, which prefer phosphatidylinositol as a substrate. Consistent with their substrate specificity, the class III PI3-kinases are the most evolutionarily ancient—they are the only class represented in every eukaryotic organism (including the simplest, yeast¹) and they are implicated in processes most ancient and fundamental to eukaryotes—vesicle trafficking processes such as endosome-to-Golgi² or lysosome¹ transport, autophagy³, and phagocytosis⁴. In contrast, the class I and II PI3-kinases have been mostly implicated in processes observed in higher organisms such as downstream transmission from growth factor receptors^{5,6}.

The structural features of the enzyme complexes of PI3-kinases similarly reflect the relative evolutionary relationship between the different classes of enzymes. Examination of the apo-structure of *Drosophila* Vps34⁷ (PDB 2X6H), which has the highly-conserved phosphoinositide binding loop fully ordered, allows the proposal of an enzymatic scheme where H745 is in proximity to a putative PI binding site and acts as a general base to promote phosphorylation of the D-3 hydroxyl group; this residue (and

the adjacent two residues) are absolutely conserved in PI3-kinases, suggesting that the proton transfer mechanism in vps34 is ancestral to the other PI3-kinases. Moreover, while the class I and class II PI3-kinases require features common to higher organisms either protein-protein adaptor accessory subunits or direct RTK interactions to activate them and recruit them to the membranes they act on, the sole class III PI3K enzyme Vps34 seems to be capable of direct recruitment to membranes of action through its myristoylated regulatory subunit Vps15⁸, a mechanism which would be useful in an ancestral organism lacking receptor tyrosine kinases.

However, despite the simpler construction and action of class III PI3K, relatively little specific detail is understood about its function in eukaryotic cells. This is due mostly to the inability to manipulate class III/Vps34 function specifically with temporal precision; Vps34 is not known to be specifically activated by convenient experimental treatments (as in growth factor manipulation of class I PI3K activity), and the inhibitors known to act on Vps34 have diverse lipid and protein kinase targets. Thus, genetic silencing manipulations can be used to remove Vps34 function and show that a specific cellular process fails, but it is difficult to ascertain the exact role of PI3K protein or enzymatic activity in a particular process. In an attempt to improve reagents available for Vps34 manipulation, we undertook a structure-based drug design survey to identify features of inhibitors that selectively inhibit Vps34⁷; the following is derived largely from this published work.

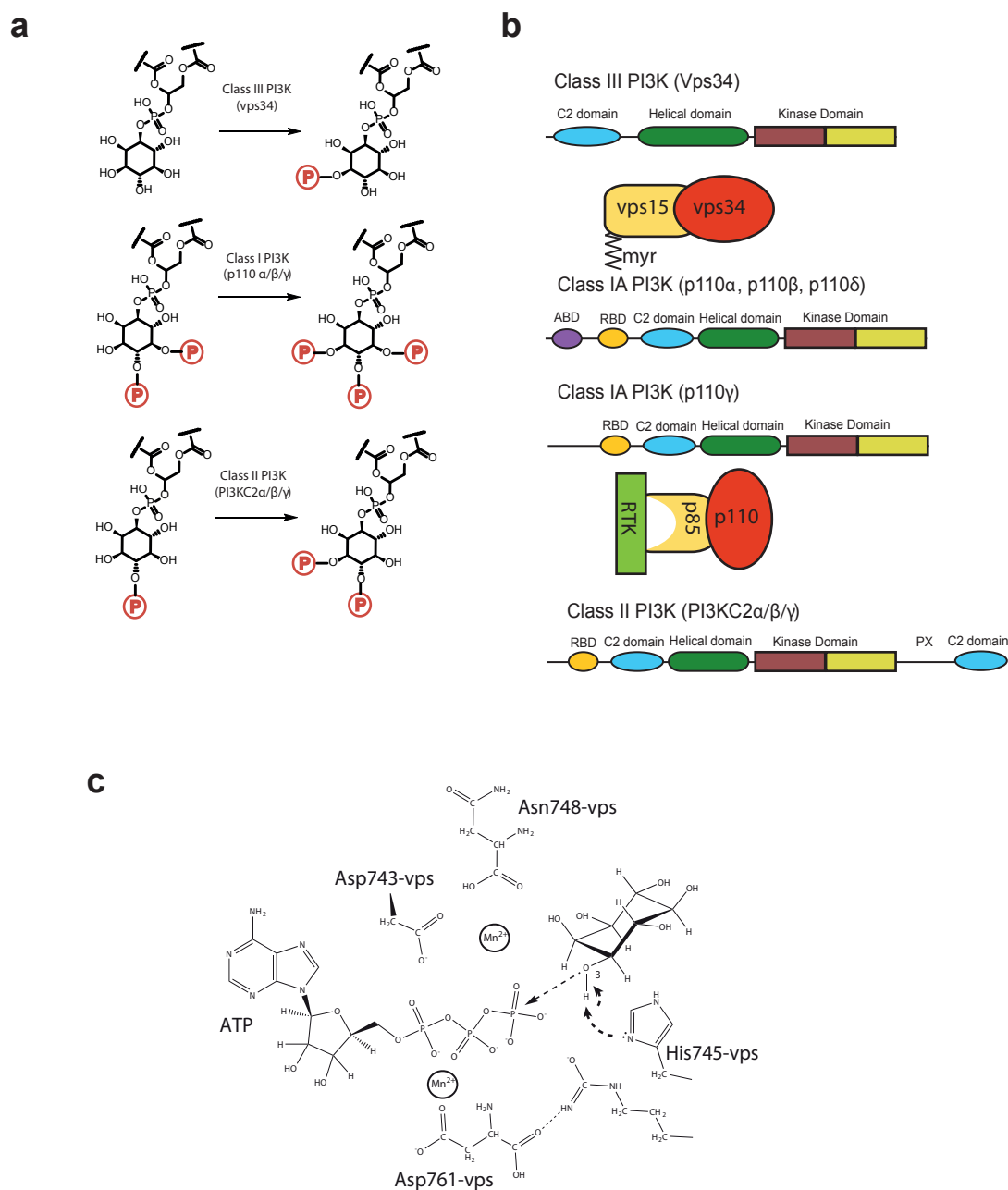


FIGURE 1. Features of PI3-kinases. *a*, substrate specificity of classes of PI3K; class III PI3K is capable of phosphorylating phosphatidylinositol whereas class I PI3K requires 4,5-bisphosphorylation of phosphatidylinositol. *b*, domain architecture of PI3K; class I, II and III PI3K share a common architecture consisting of a membrane-binding C2 domain, helical domain, and kinase domain whereas class I PI3K have additional ABD (p85 binding) and RBD (RAS binding) domains which drive interactions with accessory proteins. *c*, proposed mechanism of phosphate transfer from ATP to 3'-hydroxyl of PI; His745 of vps34 (homologous to p110a H917/p110g 948) appears to act as a general base in the reaction.

PIK-93 binding to Drosophila Vps34

Other than the commonly used PI3K inhibitors wortmannin, LY294002, and 3-methyladenine, there is little data available for Vps34 inhibition by small-molecule inhibitors. We decided to start with the compound PIK93⁹ described by Knight et al. as a PI3K/Vps34 inhibitor¹⁰. Although PIK93 inhibits p110 α and p110 γ potently (36nM and ~4nM, respectively), it also inhibits HsVps34 (36nM). To gain insight into how PIK-93 might be modified to affect its selectivity for Vps34 over other PI3K, we compared the structures of DmVps34-PIK93 (pdb code 2X6J) and Hsp110 γ -PIK93 (pdb code 2CHZ) (Figure 2).

PIK93 binds to DmVps34 in a remarkably similar conformation to that of p110 γ , with the 4-chloro substituent on the phenyl ring oriented toward the affinity pocket (Figure 2). The thiazole nitrogen and amine of PIK93 make contacts with the carbonyl oxygen and amide nitrogen of hinge residue V747 that are equivalent to the hinge binding contacts of PIK93 to the carbonyl oxygen and amide nitrogen of V882 in the structure of p110 γ -PIK93. Additionally, there may be weak H-bonding contacts between K698 and the PIK93 sulfonamide and D823 and the PIK93 ethanolamino hydroxyl. Finally, the phenylthiazole core of PIK93 is in DmVps34 flanked by I696/L744 in the N-terminal lobe and I812/I882 in the C-terminal lobe; these form a similar binding surface to the configuration in p110 γ . The broad similarity between the binding conformations for PIK93 to both kinases would tend to be consistent with the relatively potent IC50s observed (4nM and 34 nM for p110 γ and Vps34, respectively)

Inhibition of vps34 by 3-methyladenine

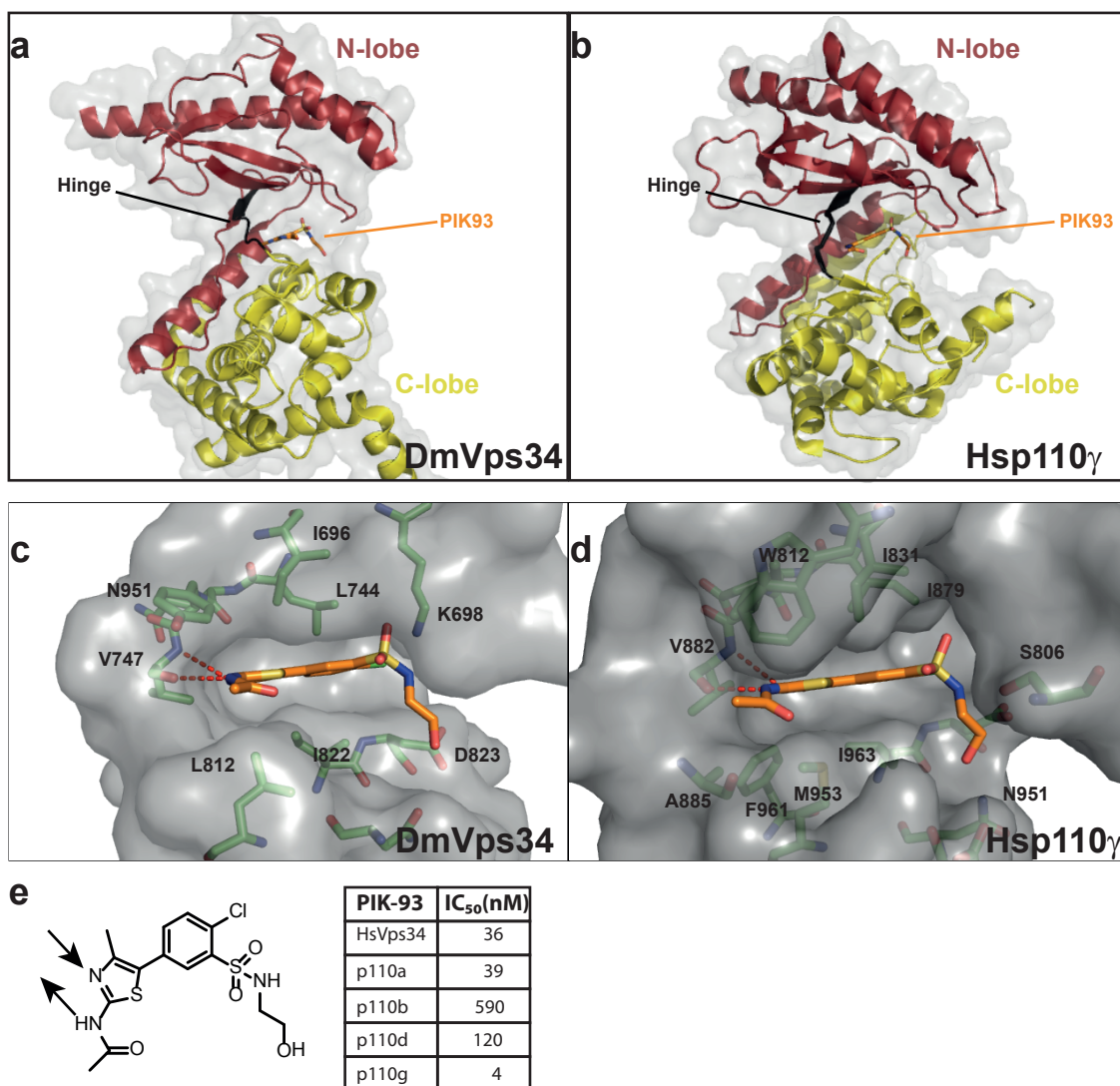


FIGURE 2. Comparison of binding mode of PIK-93 to DmVps34 (pdb code 2X6J) and Hsp110g (pdb code 2CHZ). *a*, kinase domain of Drosophila Vps34. *b*, kinase domain of Homo Sapiens p110 γ . *c*, DmVps34-PIK93; thiazole and amine nitrogens form hydrogen bonding contacts with hinge residue V747, K698 and D823 may form weak contacts with amine and hydroxyl group of ethanolamino moiety of PIK93. *d*, Hsp110 γ -PIK93; thiazole and amine nitrogens form hydrogen bonding contacts with amine and carboxyl of hinge residue V882, S806 and N951 may form weak contacts with amine and hydroxyl group of ethanolamino moiety of PIK93. *e*, structure of PIK93 and IC₅₀ values against other PI3-kinases.

Any discussion of small molecule inhibition of Vps34 should address the widely used Vps34 inhibitor 3-methyladenine. Originally identified in a screen for nucleotide analogs that would affect protein degradation without impacting protein synthesis¹¹, 3-methyladenine was found to affect endogenous but not exogenous protein degradation via reduction of autophagogenesis in hepatocytes. Later, Petiot et al.¹² discovered that this autophagic effect was similar to that of Vps34 antisense oligonucleotides and that 3-MA was a weak class III PI3K inhibitor. Since this molecule has been widely used as a tool to specifically interrogate autophagy/class III PI3K function, we figured it would be a reasonable starting point to gain insight into features that drive inhibitor selectivity for class III PI3K.

Surprisingly, we were unable to find any published data representing the affinity of 3-methyladenine for class I PI3K; accordingly, we first examined the inhibition of class I PI3-kinases p110 α and p110 γ and class III Vps34 by in vitro kinase assay using phosphatidylinositol (Figure 3c). Although 3-MA exhibits relatively low potency for all three PI3-kinases (tens to hundreds of micromolar IC₅₀s) and shows little selectivity for Vps34 over p110 γ (~2 fold), it was found to have moderate selectivity for Vps34 over p110 α (~5 fold). To see if there were any unique structural features that might be exploited by 3-MA to cause this trend that could possibly be incorporated into other inhibitors, we next examined the binding of 3-MA in the crystal structure of *Drosophila* Vps34 (pdb code 2X6F, Figure 3a). By comparison to the original structure of p110 γ -ATP, we were able to infer that 3-MA likely makes analogous hinge-binding contacts to ATP in p110 γ (residues V747 and Q745 in dm $vps34$), but utilizing two pyridine nitrogens instead of a single pyridine nitrogen and the exocyclic amine of adenine. Because of its relatively small size compared to other PI3K inhibitors, 3-MA seems to engage only a small subset of hydrophobic residues in the ATP binding site (Y746, I696, F673, L812,

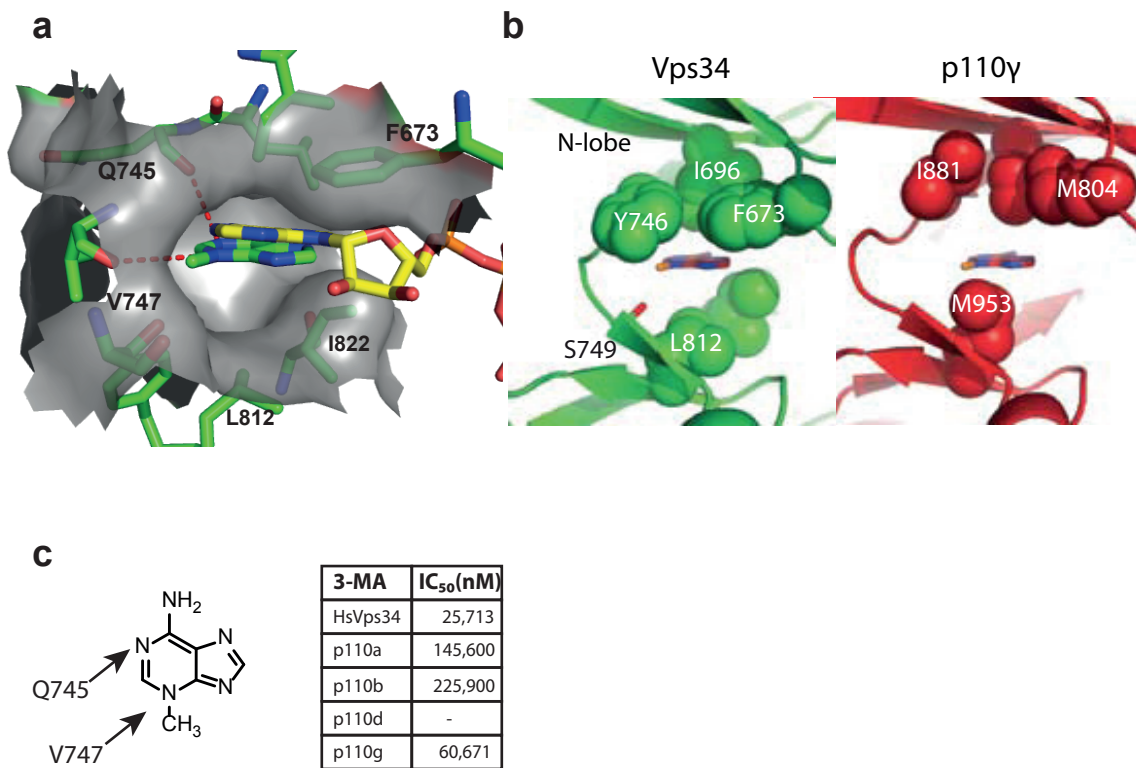


FIGURE 3. 3-Methyladenine binding to Vps34. *a*, comparison of binding orientation of 3-MA (green, pdb 2X6F) and ATP (yellow), ATP orientation is derived from pdb code 1E8X; 3-MA pyrimidine nitrogens appear to satisfy hydrogen bonds normally formed by pyrimidine nitrogen and exocyclic amine of adenine. *b*, comparison of flanking residues in vps34 and p110. *c*, in vitro IC₅₀ values of 3-MA against PI3K enzymes.

I822). These residues are not conserved in p110 γ , instead being replaced by I881/M804/M953, all of which are, surprisingly, conserved in p110 α despite the larger selectivity ratio versus p110 α . These residues may adopt a different conformation in p110 α , accounting for the difference in selectivity ratio, but this observation, combined with the fact that 3-MA utilizes similar contacts to ATP and has been observed to significantly inhibit class I PI3K in cells at standard experimental concentrations¹³ suggested to us that 3-MA is a relatively unselective inhibitor which would not yield useful insight into design of more selective Vps34 inhibitors, nor would it serve as a useful starting compound to explore new selectivity features (due to its low potency). These results would also seem to suggest that the use of 3-MA for cellular studies (especially in cells where p110 γ is the primary signaling PI3K isoform) should be interpreted with extreme caution, as any observed phenotype probably represents significant PI3K inhibition.

Differential Comparison of DmVps34 and p110 γ bound to PIK93

Because 3-MA represented a poor target for elaboration due to its low potency and similarity to ATP, we decided to attempt to elaborate PIK93 into a more specific inhibitor of HsVps34. We first started by comparing differences in the outer shell (~8 angstroms) of residues around PIK93 in the structures of DmVps34 and p110 γ bound to PIK93, looking for features present in DmVps34 conserved in HsVps34 which could be exploited to gain affinity or, alternatively, features that would tend to occlude binding to p110 γ but not Vps34.

The first obvious unique feature in the structure of Vps34 was the presence of two polar residues (K674, E752) near the “entrance” to the ATP binding pocket within ~5 angstroms of the PIK93 acetamide (Figure 4a). Although there is a lysine in p110 γ in an analogous location, it is oriented away from the binding pocket in the crystal structure. Moreover, both polar residues are conserved as K614 and E692 in HsVps34, suggesting that the acetamide portion of PIK93 might be able to be modified with a longer polar substituent to contact these residues.

The second obvious unique feature of the Vps34 structure compared to p110 γ was the conformation of the “affinity pocket” (Figure 4b). In other inhibitors of the PI3K family, filling this pocket plays an important role in driving affinity of the inhibitor for the PI3K binding site¹⁰; however, the 4-chloride substituent of PIK93 is too short to make significant contact with this binding region. However, there is a clear steric difference between the affinity pocket of the Vps34 structure and that of p110 γ , the former being much larger—suggesting that larger substituents in place of PIK93’s 4-chloride might be able to exploit steric differences between the two enzymes to derive selectivity for Vps34.

The third feature evident from the Vps34 structure was the conformation of the “hinge” region linking the N- and C-lobes of Vps34 (Figure 4c). Since ATP (as well as most kinase inhibitors) make hydrogen bonds to the polypeptide backbone in this region, it is unsurprising that the region is variable between Vps34 and p110 γ (and even between Human and Drosophila Vps34, presumably due to the lack of selective pressure). However, p110 γ has a large hydrophobic residue (W812) in the proximity of the acetamide of PIK93, which is represented by smaller/more flexible residues in the case of both Human (Q) and Drosophila (K) Vps34. This raised the possibility that a

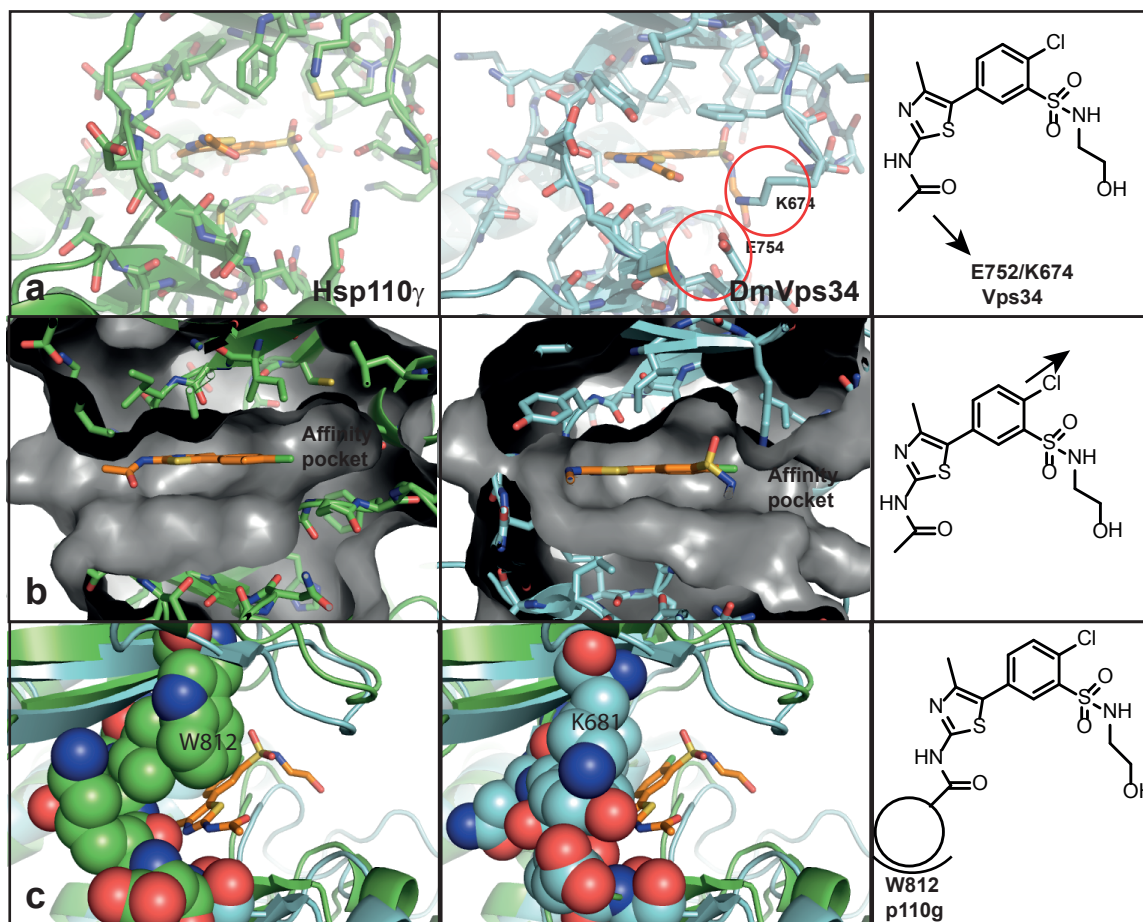


FIGURE 4. Structural differences between PIK93-Dmvps34 (pdb code 2X6J) and PIK93-Hsp110 γ (pdb code 2CHZ). a, Vps34 possesses charged residues near the front of the binding pocket which may be able to interact with polar extensions from the acetamide position of PIK93. b, affinity pocket of Vps34 appears to be larger in Vps34 structure and may accommodate larger substituents on the phenyl ring in place of the 4-chloride. c, hinge binding region of Vps34 is less occluded than that of p110 γ due to a W->K substitution (or an analogous W->Q substitution in HsVps34); bulkier substituents in the acetamide position may be accommodated by vps34 but not p110 γ .

bulkier/branched substituent in the acetamide region could preclude binding to p110 γ while preserving binding to either of the Vps34 orthologs.

Synthesis and Evaluation of PIK93 Analogs

The proposed changes to PIK93 to generate new analogs involved either a) modifying the para-substituent of the phenyl ring or b) modifying the acyl group attached to the aminothiazole. The former could be accomplished simply by using 4-bromo- or 4-methoxyphenylacetone in place of 4-chlorophenylacetone in the first synthetic step to yield those corresponding derivatives. To simplify the synthesis, however, we desired a way to incorporate the second amide modification divergently—which could theoretically be accomplished by reacting the substituted alpha-bromo ketones with acyl thioureas (Figure 5a) to generate phenylthiazoles with both modifications. Initial attempts to generate the acylthioureas by reaction of thiocyanate with acid chlorides followed by ammonia addition were unsuccessful; however, refluxing substituted acyl chlorides with thiourea in dry toluene overnight successfully yielded the desired compounds, presumably via a mechanism involving an S- to N- shift.

Replacing the chloride of PIK93 with bromide, the acetamide with propionamide, or the aminoethanol group with aminopropanol had very little effect on inhibitor binding to either Vps34 or p110 γ , as the corresponding inhibitors 3-92A, 3-92B, 3-94B, and 3-94C have similar potency against both targets to PIK93 (Figure 4b). Disappointingly, even the addition of methyl 4-oxobutanoate in the acetamide position (which was designed to interact with the polar residues K614 and E692, Figure 4a) had almost no effect on binding, which was surprising considering the much greater bulk of that substituent.

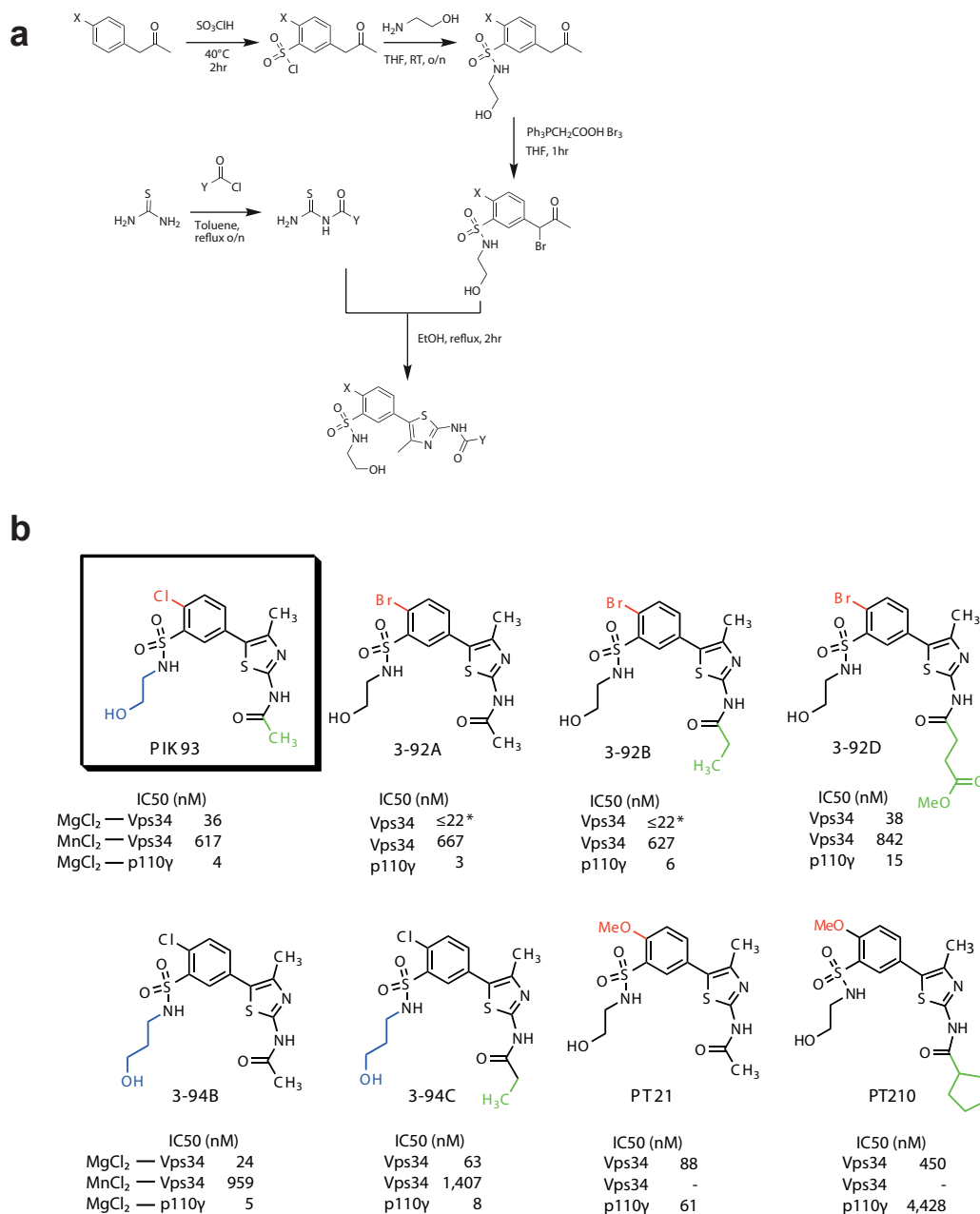


FIGURE 5. Synthesis of PIK93 analogs. a, synthetic scheme for PIK93 analogs. b, in vitro IC₅₀ values for PIK93 analogs against Vps34 and p110g. * In the case of some inhibitors, their IC₅₀ value approached the accurate limit of determination in the assay with Mg²⁺ as cofactor (~22nM). Thus, the IC₅₀ values for these compounds were also measured with Mn²⁺. IC₅₀ values measured with Mn²⁺ are approximately 10-20-fold higher than those measured with the physiologically more abundant divalent metal Mg²⁺, because the enzyme is more active with the Mn²⁺ cofactor. Substitution of a cyclopentanecarboxamide in PT210 for the acetamide moiety of PIK-93 reverses the specificity of the compound.

However, increasing the steric bulk of the phenyl substituent from chloride to methoxide (PT21, Figure 5) finally yielded a significant effect on binding, decreasing affinity for both enzymes but switching the specificity of the inhibitor such that it targeted both enzymes roughly equally (88nM for Vps34 vs 61 nM for p110 γ); presumably this modification exploits differences in the shape of the Vps34 affinity pocket (figure 4b). Moreover, combining this modification with a branched cyclopentane substituent in the acetamide position (predicted to clash with the bulkier hinge region of p110 γ , Figure 3c) yielded an inhibitor with moderate (~5 fold) selectivity for Vps34 (450 nM) over p110 γ (4,428 nM).

Ultimately, our attempts to produce more Vps34-selective analogs of PIK93 indicate that it is likely possible to produce higher-affinity selective inhibitors for Vps34. Although all the modifications we employed either had neutral or deleterious effects on binding, the PT21 and PT210 compounds demonstrate that there are structural “selectivity filters” of Vps34 that can be exploited to drive selectivity for the enzyme. Furthermore, the neutral effect of the other modifications demonstrate that there is ample room to further elaborate the acetamide and sulfonamide portions of the PIK93 scaffold; in particular, additional polar modifications in the acetamide position (amino acid amides, for example) may prove more fruitful in enhancing selectivity for Vps34, as interaction with the K614/E692 residues is likely geometrically constrained.

The identification of the cyclopentanecarboxamide/4-methoxy substitutions as an apparent selectivity filter for Vps34 also suggests further strategies for non structure-guided inhibitor development. Although the only sulfonamide substituents we examined here were aminoalcohols, the structure of both p110 γ and Vps34 suggest that substituents of different shape may be accommodated in that position (Figure 2). It is

possible that exploration of diverse substitution in that region may uncover differences between Vps34 and p110 γ not immediately obvious from the static crystal structures.

Experimental Methods

Inhibitor Assay of p110 α /p110 β /p110 γ /HsVps34

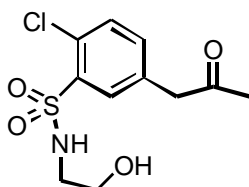
Assays of p110 α /p110 β /p110 γ were performed with L α -phosphatidylinositol (Avanti) as described in Knight et al. Nat Protoc. 2007;2(10):2459-66. Inhibitor series were prepared 10% DMSO as 5x stocks for the assay.

Assays of HsVps34 were performed as described in Knight et al, except that the final assay buffer composition used was changed to 20mM HEPES 7.5, 100 mM NaCl, 3 mM MgCl, 1mg/mL PI and 44nM hvps34 was used in the assay. For inhibitors with an apparent IC₅₀ less than or equal to 22nM, values were reassayed using 4.4nM hvps34 with 3 mM MnCl₂.

Synthesis of PIK-93 analogs

Synthesis of PIK-93 is reported in Knight et al. Cell, Volume 125, Issue 4, 733-747. Reproduced here for completeness as products 1-3.

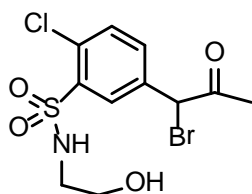
(1) 2-chloro-N-(2-hydroxyethyl)-5-(2-oxopropyl)benzenesulfonamide



1-(4-chlorophenyl)propan-2-one (1 mL, 14.8 mmol) was added dropwise to SO₃ClH (5 mL) in an ice bath, and the reaction was then heated to 40° C for 2 hours. The reaction was stopped by transfer dropwise to 200 mL ice. The aqueous phase was then extracted 3 times with EtOAc, the combined organic dried with Na₂SO₄, filtered, and then concentrated *in vacuo* to give a brown oil. This oil was dissolved in THF (10mL), ethanolamine was added (~1.5 mL), and the reaction was allowed to stir overnight at room temperature. The following day the reaction was concentrated *in vacuo*, water was added, and the aqueous phase was extracted three times with EtOAc. The combined organic phase was concentrated, and the product purified by silica gel flash chromatography using a gradient of 2% - 10% MeOH in CH₂Cl₂. The product containing fractions from this column were combined, solvent removed *in vacuo*, and the product was subjected to a second purification by reverse phase HPLC using a MeCN/H₂O/0.1% TFA solvent system. Product containing fractions were lyophilized to yield 414 mg (24% yield) of product. LC-ESIMS

[MH]⁺ m/z calcd for C₁₁H₁₅ClNO₄S, 292.03; found, 292.17.

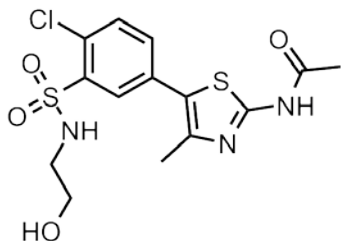
(2) 5-(1-bromo-2-oxopropyl)-2-chloro-N-(2 hydroxyethyl)benzenesulfonamide



Ph₃PCH₂CH₂COOH Br₃ (900 mg, 1.5 mmol) was dissolved in THF (15 mL) (Armstrong et al., 1975). Product 7 (414 mg, 1.42 mmol) was dissolved in THF (10 mL) and this was added dropwise to the first solution at room temperature. The reaction was allowed to proceed one hour at room temperature, at which

point the solvent was removed *in vacuo* and the product purified by silica gel flash chromatography to yield 377 mg (72% yield) of product. LC-ESI-MS [MH]⁺ m/z calcd for C₁₁H₁₄BrClNO₄S, 369.94; found, 369.83.

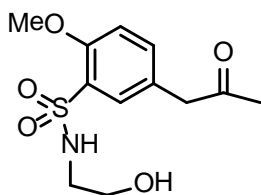
(3) PIK-93 (N-(5-(4-chloro-3-(N-(2-hydroxyethyl)sulfamoyl)phenyl)-4-methylthiazol-2-yl)acetamide)



Product 8 (377 mg, 1.02 mmol) was dissolved in ethanol (6 mL), and N-acetylthiourea (130 mg, 1.1 mmol) was added at room temperature. The reaction was heated to reflux for 30 minutes, then cooled to room temperature, and the product purified by silica gel flash chromatography using a gradient of 0% - 10%

MeOH in CH₂Cl₂ to yield 167 mg (42% yield) of PIK-93. LC-ESI-MS [MH]⁺ m/z calcd for C₁₄H₁₇ClN₃O₄S₂, 390.03; found, 390.14.

(4) N-(2-hydroxyethyl)-2-methoxy-5-(2-oxopropyl)benzenesulfonamide

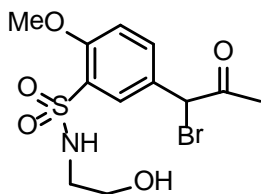


1-(4-methoxyphenyl)propan-2-one (2mL, 13 mmol) was added dropwise to 10mL SO₃ClH cooled on a dry ice ethanol/ethylene glycol (1:9) bath over 5 minutes. The reaction was allowed to stir for 30 minutes, warmed to room temperature and allowed to

stir for 2 hours. The reaction was then cooled on ice and quenched by dropwise addition to 200mL ice/water with stirring. Once the ice had melted, the reaction was extracted 3x with ethyl acetate. The combined organic layers were dried with brine and sodium sulfate and reduced in vacuo. The residue was dissolved in 10mL dry THF and added dropwise to a solution of 1.5 mL ethanolamine in 10mL THF. The reaction was allowed to stir overnight and then reduced in vacuo. 50 mL water was added, and the aqueous layer was extracted 3x with ethyl acetate. The combined ethyl acetate was dried with brine and sodium sulfate, reduced in vacuo, and purified by flash chromatography in 0-10% methanol in dichloromethane. Yield 0.8 g (21%).

LC-ESIMS [MH]⁺ m/z calcd for C₁₂H₁₇NO₅S, 288.08; found 287.94.

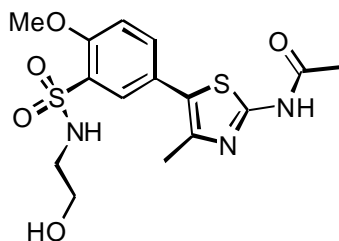
(5) 5-(1-bromo-2-oxopropyl)-N-(2-hydroxyethyl)-2-methoxybenzenesulfonamide



Synthesis was performed as in (2), substituting (4) for (1). Compound was purified by silica flash chromatography in ethyl acetate. Yield 0.82g (80%).

LC-ESIMS [MH]⁺ m/z calcd for C₁₂H₁₆BrNO₅S, 365.99; found 365.79.

(7) PT-21 (N-(5-(3-(N-(2-hydroxyethyl)sulfamoyl)-4-methoxyphenyl)-4-methylthiazol-2-yl)acetamide)

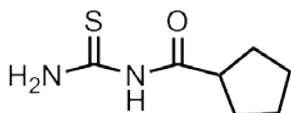


Product (5) (100mg, 0.28 mmol) was dissolved in ethanol (2 mL), and N-acetylthiourea (35mg, 0.3 mmol) was added. The reaction was heated to reflux for 1 hour, reduced in vacuo, and the residue was purified by flash chromatography in a gradient of 0-10% methanol in dichloromethane. Yield 57 mg (53%).

$^1\text{H NMR}$ (400 MHz, DMSO) δ 7.72 (d, $J = 2.3$, 1H), 7.67 (dd, $J = 8.5, 2.2$, 1H), 7.30 (d, $J = 8.7$, 1H), 7.18 (s, 1H), 4.64 (s, 1H), 3.93 (s, 3H), 3.35 (dd, $J = 12.3, 6.3$, 2H), 2.85 (dd, $J = 12.5, 6.3$, 2H), 2.49 (m, DMSO), 2.31 (s, 3H), 2.13 (s, 3H).

LC-ESI-MS $[\text{MH}]^+$ m/z calcd for $\text{C}_{15}\text{H}_{19}\text{N}_3\text{O}_5\text{S}_2$, 386.08; found 385.94.

(8) N-carbamothioylcyclopentanecarboxamide

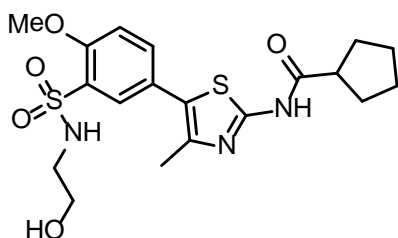


Cyclopentanecarboxylic acid (1.48g, 13 mmol) was treated with oxalyl chloride (1.65g, 32.5 mmol) by stirring in a dry, argon-purged flask at room temperature for 30 minutes and then refluxing at 72 degrees for 1 hour. Dry toluene (26mL) and ethanol-recrystallized thiourea (5g, 65.7mmol) was added. The reaction was heated to reflux

and allowed to stir for 18 hours. Toluene was then removed in vacuo and the reaction was diluted in 200mL ethyl acetate and filtered. The organic layer was washed 2x with water and dried with brine and sodium sulfate before reducing in vacuo. The compound was adsorbed onto silica and purified by silica flash chromatography using 25% ethyl acetate in hexanes. Yield 1.28g (57%).

LC-ESIMS [MH]⁺ m/z calcd for C₇H₁₂N₂O₅S, 173.07; found 172.92.

(9) PT210 (N-(5-(3-(N-(2-hydroxyethyl)sulfamoyl)-4-methoxyphenyl)-4-methylthiazol-2-yl)cyclopentanecarboxamide)

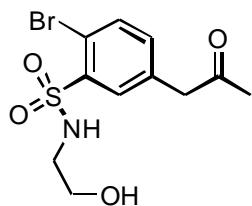


Product (5) (100mg, 0.274 mmol) was dissolved in ethanol (2 mL), and (8) (47mg, 0.300 mmol) was added. The reaction was heated to reflux for 1 hour, reduced in vacuo, and the residue was purified by flash chromatography in a gradient of 0-10% methanol in dichloromethane. Yield 90 mg (75%).

¹H NMR (400 MHz, DMSO) δ 7.72 (s, 1H), 7.65 (m, 1H), 7.30 (d, J = 8.6, 1H), 7.18 (m, 1H), 3.89 (m, 3H), 3.7 (broad, H₂O), 3.36 (m, 2H), 2.85 (m, 2H), 2.49 (m, DMSO), 2.31 (s, 1H), 1.86 (m, 2H), 1.67 (m, 4H), 1.5-2.9 (m, broad, 6H).

LC-ESI-MS [MH]⁺ m/z calcd for C₁₉H₂₅N₃O₅S₂, 440.12; found 440.4.

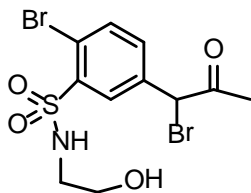
(10) 2-bromo-N-(2-hydroxyethyl)-5-(2-oxopropyl)benzenesulfonamide



1-(4-bromophenyl)propan-2-one (2mL, 13mmol) was added dropwise to 10mL SO₃ClH cooled on a dry ice ethanol/ethylene glycol (1:9) bath over 5 minutes. The reaction was allowed to stir for 30 minutes, warmed to room temperature, and heated at 40 degrees for 2 hours. The reaction was cooled on ice and quenched by dropwise addition to 200mL ice/water with stirring. Once the ice had melted, the reaction was extracted 3x with ethyl acetate. The combined organic layers were dried with brine and sodium sulfate and reduced in vacuo. The residue was dissolved in 10mL dry THF and added dropwise to a solution of 1.5 mL ethanolamine in 10mL THF. The reaction was allowed to stir overnight and then reduced in vacuo. 50 mL water was added, and the aqueous layer was extracted 3x with ethyl acetate. The combined ethyl acetate was dried with brine and sodium sulfate, reduced in vacuo, and purified by flash chromatography in 0-10% methanol in dichloromethane. The product containing fractions from this column were combined, solvent removed *in vacuo*, and the product was subjected to a second purification by reverse phase HPLC using a MeCN/H₂O/0.1% TFA solvent system. Yield 0.248 g (5.6%).

LC-ESI-MS [MH]⁺ m/z calcd for C₁₁H₁₄BrNO₄S, 335.98; found 335.8.

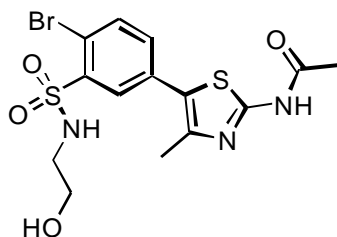
(11) 2-bromo-5-(1-bromo-2-oxopropyl)-N-(2-hydroxyethyl)benzenesulfonamide



Product (10) (0.248g, 0.737mmol) in 10mL THF was added dropwise to Ph₃PCH₂CH₂COOH Br₃ (0.442g, 0.737 mmol) in 10mL THF. The reaction was allowed to stir for 1 hour at room temperature. Ethyl acetate (~5mL) was added, and the reaction was filtered and reduced in vacuo. The product was used without further purification. Yield 0.25 g (82%).

(12) 92A (N-(5-(4-bromo-3-(N-(2-hydroxyethyl)sulfamoyl)phenyl)

-4-methylthiazol-2-yl)acetamide)

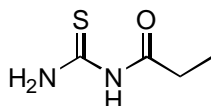


Product (11) (50 mg, 0.120 mmol) was dissolved in 5mL dry ethanol and N-acetylthiourea (15.6mg, 0.132mmol) was added. The reaction was refluxed for 1 hr and the ethanol was removed in vacuo. The residue was resuspended in 1mL DMSO and purified by reverse phase HPLC using a MeCN/H₂O/0.1% TFA solvent system. Yield 15 mg (29%).

¹H NMR (400 MHz, DMSO) 7.97 (d, J = 2.3, 1H), 7.88 (d, J = 8.3, 2H), 7.59 (d, J = 8.3, 1H), 3.95 (broad), 3.39 (t, J = 6.4, 2H), 2.95 (d, J = 6.0, 2H), 2.49 (m, DMSO), 2.36 (s, 3H), 2.15 (s, 3H).

LC-ESI-MS [MH]⁺ m/z calcd for C₁₄H₁₆BrN₃O₄S₂, 433.98; found 433.79.

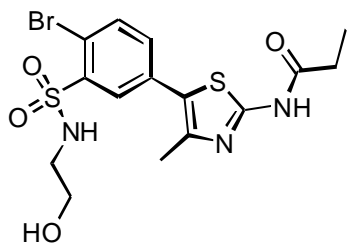
(13) N-carbamothioylpropionamide



To ethanol-recrystallized thiourea (1.0g, 13.1 mmol) in 13 mL dry toluene was added 1.14 mL (13.1mmol) propionyl chloride. The reaction was heated to reflux for 16 hours, and then toluene was removed in vacuo. The product was recrystallized from ethanol to yield 0.8g product (46%).

LC-ESI-MS [MH]⁺ m/z calcd for C₄H₈N₂OS, 133.04; found 132.89.

(14) 92B (N-(5-(4-bromo-3-(N-(2-hydroxyethyl)sulfamoyl)phenyl)-4-methylthiazol-2-yl)propionamide)

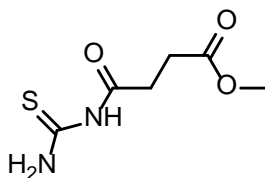


Product (11) (50 mg, 0.120 mmol) was dissolved in 5mL dry ethanol and product (13) (17.5mg, 0.132mmol) was added. The reaction was refluxed for 1 hr and the ethanol was removed in vacuo. The residue was resuspended in 1mL DMSO and purified by reverse phase HPLC using a MeCN/H₂O/0.1% TFA solvent system. Yield 10mg (19%).

¹H NMR (400 MHz, DMSO) δ 7.97 (s, 1H), 7.88 (d, J = 8.3, 1H), 7.59 (d, J = 8.3, 1H), 4.19 (broad), 3.39 (t, J = 6.4, 2H), 2.95 (m, 2H), 2.49 (m, DMSO), 2.44 (d, J = 7.5, 2H), 2.36 (s, 3H), 1.09 (m, 3H).

LC-ESI-MS [MH]⁺ m/z calcd for C₁₅H₁₈BrN₃O₄S₂, 447.99; found 447.81.

(15) Methyl 4-oxo-4-thioureidobutanoate

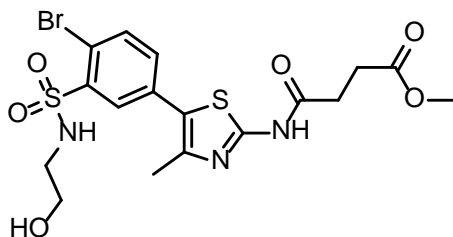


Methyl 4-chloro-4-oxobutanoate (2.93 mL, 23.9 mmol) was added dropwise to thiourea (2.0 g, 26.3 mmol) in 30 mL dry toluene. The reaction was heated to reflux for 18 hours,

then toluene was removed in vacuo. The residue was dissolved in 200mL ethyl acetate, washed 3x with brine, dried with sodium sulfate, and reduced in vacuo. The dry product was adsorbed onto silica and purified by flash chromatography in 50% ethyl acetate in hexanes. Yield 1.0 g (22%).

LC-ESI-MS [MH]⁺ m/z calcd for C₆H₁₀N₂O₃S, 191.04; found 191.3.

(16) 92D (Methyl 4-(5-(4-bromo-3-(N-(2-hydroxyethyl)sulfamoyl)phenyl)-4-methylthiazol-2-ylamino)-4-oxobutanoate)

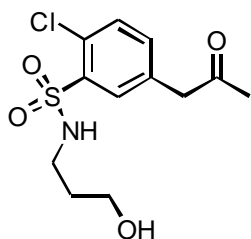


Product (11) (50 mg, 0.120 mmol) was dissolved in 5mL dry ethanol and product (15) (25.2mg, 0.132 mmol) was added. The reaction was refluxed for 1 hr and the ethanol was removed in vacuo. The residue was resuspended in 1mL DMSO and purified by reverse phase HPLC using a MeCN/H₂O/0.1% TFA solvent system. Yield 11 mg (18%).

¹H NMR (400 MHz, DMSO) δ 7.97 (s, 1H), 7.88 (m, 1H), 7.59 (m, 1H), 3.7 (broad), 3.59 (d, J = 2.6, 3H), 3.39 (m, 2H), 2.95 (m, 2H), 2.72 (m, 2H), 2.64 (m, 2H), 2.49 (m, DMSO), 2.37 (s, 3H).

LC-ESI-MS [MH]⁺ m/z calcd for C₁₇H₂₀BrN₃O₆S₂, 505.99; found 505.77.

(17) 2-chloro-N-(3-hydroxypropyl)-5-(2-oxopropyl)benzenesulfonamide

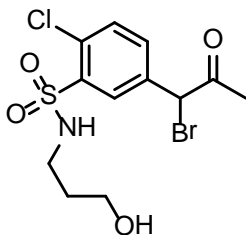


1-(4-chlorophenyl)propan-2-one (1mL) was added dropwise to 5mL SO₃ClH cooled on a dry ice ethanol/ethylene glycol (1:9) bath over 5 minutes. The reaction was allowed to stir for 30 minutes, warmed to room temperature and heated to 40 degrees Celsius for 2 hours. The reaction was then cooled on ice and quenched by dropwise addition to 200mL ice/water with stirring. Once the ice had melted, the reaction was extracted 3x with ethyl acetate. The combined organic layers were dried with brine and sodium sulfate and reduced in vacuo. The residue was dissolved in 10mL dry THF and added dropwise to a solution of 2.0 mL 3-aminopropan-1-ol in 10mL THF. The reaction was allowed to stir overnight and then reduced in vacuo. 50 mL water was added, and the aqueous layer was extracted 3x with ethyl acetate. The combined ethyl acetate was dried with brine and sodium sulfate, reduced in vacuo, and purified by flash chromatography in 0-10% methanol in dichloromethane. The product containing fractions from this column were combined, solvent removed *in vacuo*, and the product

was subjected to a second purification by reverse phase HPLC using a MeCN/H₂O/0.1% TFA solvent system. Yield 83 mg.

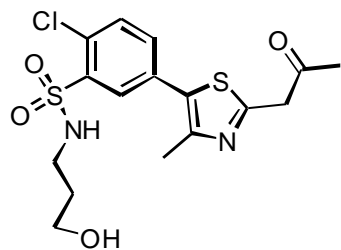
LC-ESI-MS [MH]⁺ m/z calcd for C₁₂H₁₆ClNO₄S, 306.05; found 306.3.

(18) 5-(1-bromo-2-oxopropyl)-2-chloro-N-(3-hydroxypropyl)benzenesulfonamide



Product (17) (83mg, 0.236 mmol) in 10mL THF was added dropwise to Ph₃PCH₂CH₂COOH Br₃ (0.142g, 0.236mmol) in 10mL THF. The reaction was allowed to stir for 1 hour at room temperature. Ethyl acetate (~5mL) was added, and the reaction was filtered and reduced in vacuo. The product was used without further purification. Yield 92 mg (100%).

(19) 94B (N-(5-(4-chloro-3-(N-(3-hydroxypropyl)sulfamoyl)phenyl)-4-methylthiazol-2-yl)acetamide)

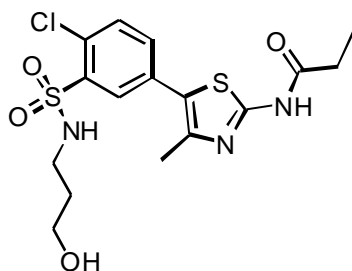


Product (18) (46 mg, 0.120 mmol) was dissolved in 5mL dry ethanol and N-acetylthiourea (15.6mg, 0.132mmol) was added. The reaction was refluxed for 1 hr and the ethanol was removed in vacuo. The residue was purified by reverse phase HPLC using a MeCN/H₂O/0.1% TFA solvent system. Yield 8 mg (16%).

¹H NMR (400 MHz, DMSO) δ 7.93 (m, 1H), 7.90 (m, 1H), 7.70 (s, 1H), 4.25 (broad), 3.35 (m, 2H), 2.93 (m, 2H), 2.49 (m, DMSO), 2.36 (d, J = 1.9, 3H), 2.15 (d, J = 1.9, 3H), 1.54 (m, 2H).

LC-ESI-MS [MH]⁺ m/z calcd for C₁₅H₁₈ClN₃O₄S₂, 404.04; found 403.88.

(20) 94C (N-(5-(4-chloro-3-(N-(3-hydroxypropyl)sulfamoyl)phenyl)-4-methylthiazol-2-yl)propionamide)



Product (18) (46 mg, 0.120 mmol) was dissolved in 5mL dry ethanol and product (13) (17.4mg, 0.132mmol) was added. The reaction was refluxed for 1 hr and the ethanol was removed in vacuo. The residue was purified by reverse phase HPLC using a MeCN/H₂O/0.1% TFA solvent system. Yield 10mg (20%).

¹H NMR (400 MHz, DMSO) δ 7.94 (m, 1H), 7.90 (m, 1H), 7.71 (s, 1H), 4.08 (broad), 3.35 (m, 2H), 2.93 (m, 2H), 2.49 (m, DMSO), 2.43 (m, 2H), 2.36 (s, 3H), 1.54 (m, 2H), 1.09 (t, J = 7.5, 3H).

LC-ESI-MS [MH]⁺ m/z calcd for C₁₆H₂₀ClN₃O₄S₂, 418.06; found 417.90.

References

1. Schu, P.V. et al. Phosphatidylinositol 3-kinase encoded by yeast VPS34 gene essential for protein sorting. *Science (New York, N.Y.)* **260**, 88-91(1993).
2. Burda, P. et al. Retromer function in endosome-to-Golgi retrograde transport is regulated by the yeast Vps34 PtdIns 3-kinase. *Journal of cell science* **115**, 3889-3900(2002).
3. Simonsen, A. & Tooze, S.A. Coordination of membrane events during autophagy by multiple class III PI3-kinase complexes. *The Journal of cell biology* **186**, 773-782(2009).
4. Vergne, I. et al. Mechanism of phagolysosome biogenesis block by viable *Mycobacterium tuberculosis*. *Proceedings of the National Academy of Sciences of the United States of America* **102**, 4033-4038(2005).
5. Arcaro, A. et al. Class II phosphoinositide 3-kinases are downstream targets of activated polypeptide growth factor receptors. *Molecular and cellular biology* **20**, 3817-30(2000).
6. Katso, R. et al. Cellular function of phosphoinositide 3-kinases: implications for development, homeostasis, and cancer. *Annual review of cell and developmental biology* **17**, 615-75(2001).
7. Miller, S. et al. Shaping development of autophagy inhibitors with the structure of the lipid kinase Vps34. *Science (New York, N.Y.)* **327**, 1638-42(2010).

8. Yan, Y. et al. hVps15, but not Ca²⁺/CaM, is required for the activity and regulation of hVps34 in mammalian cells. *The Biochemical journal* **417**, 747-755(2009).
9. BRUCE, I. (GB) et al. 5-Phenylthiazole Derivatives and Use as PI3 Kinase Inhibitors. (2003).at
<<http://www.wipo.int/pctdb/en/wo.jsp?WO=2003072557&IA=EP2003002036&DISPLAY=STATUS>>
10. Knight, Z. a et al. A pharmacological map of the PI3-K family defines a role for p110alpha in insulin signaling. *Cell* **125**, 733-47(2006).
11. Seglen, P.O. & Gordon, P.B. 3-Methyladenine: specific inhibitor of autophagic/lysosomal protein degradation in isolated rat hepatocytes. *Proceedings of the National Academy of Sciences of the United States of America* **79**, 1889-92(1982).
12. Petiot, A. Distinct Classes of Phosphatidylinositol 3' -Kinases Are Involved in Signaling Pathways That Control Macroautophagy in HT-29 Cells. *Journal of Biological Chemistry* **275**, 992-998(2000).
13. Wu, Y.-T. et al. Dual role of 3-methyladenine in modulation of autophagy via different temporal patterns of inhibition on class I and III phosphoinositide 3-kinase. *The Journal of biological chemistry* **285**, 10850-61(2010).

CHAPTER 2: DEVELOPMENT OF PHENYLTHIAZOLE INHIBITORS FOR PHOSPHOINOSITOL 4-KINASES

Biological Roles of Phosphatidylinositol 4-Kinases

Phosphatidylinositol kinases play critical roles in intracellular signaling and organization in eukaryotes, phosphorylating membrane bound phosphatidylinositol to produce second-messenger PIPs that serve as membrane anchoring sites for a wide variety of proteins bearing lipid-binding domains as well as precursors for soluble inositol polyphosphates. Probably the best understood of this class of enzymes are the class I phosphatidylinositol-3-kinases, which produce plasma membrane PI(3,4,5)P₃ (PIP₃) from PI(4,5)P₂ (PIP₂) in response to tyrosine kinase or GPCR activation and are necessary for mitogenic responses to growth factors, glucose uptake in response to insulin, and tumorigenesis in a subset of cancers¹.

Class III Phosphatidylinositol 4-kinases, despite the fact that they share significant sequence identity in their kinase domains (~67%)², and are (like the class I PI3K) sensitive to the widely used pharmacologic agent wortmannin, have been much less well studied than class I PI3K. A simplistic chemical view would predict that they play a role in the regulation of cellular levels of the substrate PI(4,5)P₂ for growth factor signaling by PI3K or phospholipase C/calcium signaling; and indeed, deletion of either isoform of PI4KIII in yeast results in an up to 50% decrease in cellular PIP₂ levels³ and inhibitors of PI4KIII α impair replenishment of PIP₂ upon hormone stimulation⁴. However, these enzymes are predominantly localized at the golgi apparatus (PI4KIIIb) or

ER (PI4KIII α) where PIP2 is absent in mammals, suggesting some role independent of receptor-stimulated plasma membrane signaling.

More consistent with this intracellular localization, recent studies on the class III PI4K have begun to implicate them and their direct product, PI(4)P, as important for controlling intracellular organization (rather than receptor signaling) in the cell. Bruns et al.⁵ demonstrated that expression of a dominant-negative version of PI4KIII β inhibited intra-Golgi transport of influenza hemagglutinin, suggesting that PI4P is necessary for delivery of a subset of protein cargoes. Furthermore, inactivation of PI4KIII β has been shown to inhibit metabolism of ceramide via impaired localization of its transport protein CERT⁶, and the presence of PX domains with selectivity for PI4P in other lipid transport proteins⁷ suggests that the enzyme may be broadly important for controlling lipid transport and membrane compartment homeostasis within the cell. Perhaps consistent with these already observed behaviors, even more recently two independent screens^{8,9} have demonstrated that both PI4KIII α and PI4KIII β are necessary host factors for establishing and/or maintaining hepatitis C replication in cultured hepatocytes. This is likely related to the mechanism by which class III PI4K controls Golgi cargo transport in the cell, as replication of the evolutionarily similar virus CVB3 shows similar dependence on both class III PI4K and the Golgi-localized PI4K effector Arf1¹⁰.

This novel data regarding the intracellular roles of class III PI4K suggests that chemical inhibitors would be useful agents for modifying lipid metabolism or infection by plus-strand RNA viruses in animals. However, development of agents for this purpose has been hampered by two issues: a) few scaffolds with potency for class III PI4K have been identified, and b) of those that have (wortmannin and PIK93)¹¹ inhibit class I PI3K in addition to class III PI4K, in addition to various protein tyrosine kinases. While this may be acceptable in therapeutics intended for cancer chemotherapy, the critical role of

receptor tyrosine kinases and class I PI3K in cell proliferation and insulin response in animals suggests that use of such nonspecific agents would induce insulin tolerance and interfere with tissue maintenance in animals.

Development of PI4K Inhibitors

We began optimization of PI4K inhibition with the 5-phenylthiazole inhibitor PIK-93, which had been previously shown to inhibit PI4KIII α and PI4K III β ¹¹ and reported to have activity against HCV replication in vitro^{8,10}. Having observed previously that substitution of the acetamide and 4-chloride regions of the PIK93 phenylthiazole scaffold could modulate inhibitor selectivity for lipid kinases, we synthesized a set of compounds replacing the acetamide with larger alkyl substituents and the 4-chloride with 4-methoxy (Figure 1). As PIK93 was originally developed as a PI3K inhibitor and because we expected that PI3K inhibition might interfere significantly with therapeutic usage of PI4K inhibitors, we screened the phenylthiazole set against PI3K p110 α and p110 γ in addition to PI4KIII α /III β for in vitro activity.

Much to our delight, two of the synthesized inhibitors appeared to be selective inhibitors of PI4KIII β (figure 1): PT19, which showed 68-fold selectivity for PI4KIII β over p110 γ and at least 400-fold selectivity versus p110 α ; and PT110, which showed which showed 27-fold selectivity for PI4KIII β over p110 γ and 48-fold selectivity versus p110 α . This being similar (but more dramatic) than the phenomenon observed with Vps34 and acetamide-substituted phenylthiazoles¹², we wondered if it might have a similar rationale—that PI4KIII β has a substitution of the W812 residue found in PI3K for a more flexible residue, allowing binding of the bulkier trimethylacetyl and

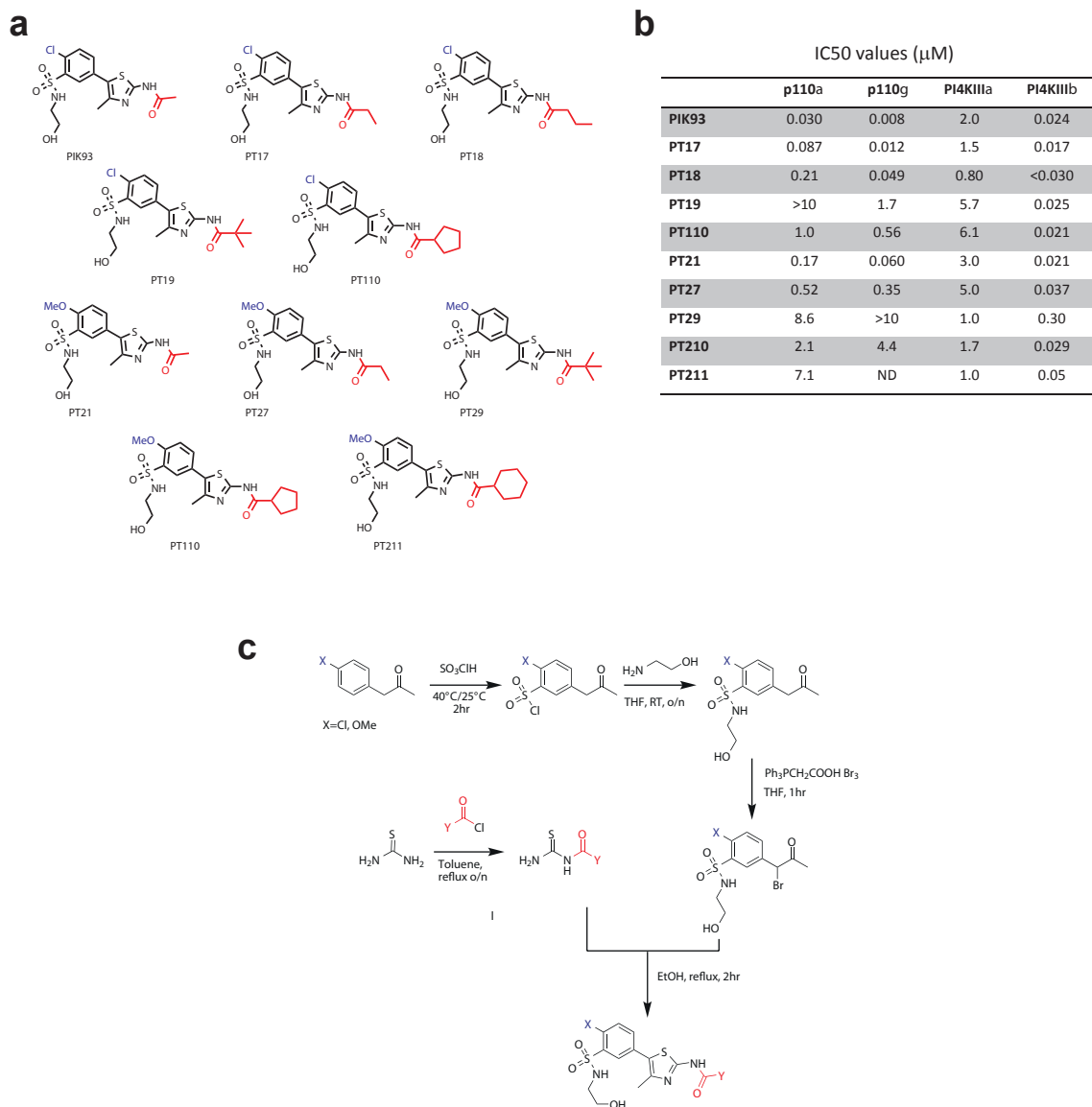


FIGURE 1. Inhibition of p110 α , p110 γ , PI4KIII α and PI4KIII β by 5-phenylthiazole panel. a, structures of phenylthiazole inhibitors. b, IC₅₀ values (μM) against lipid kinases. c, synthetic scheme for phenylthiazole inhibitors.

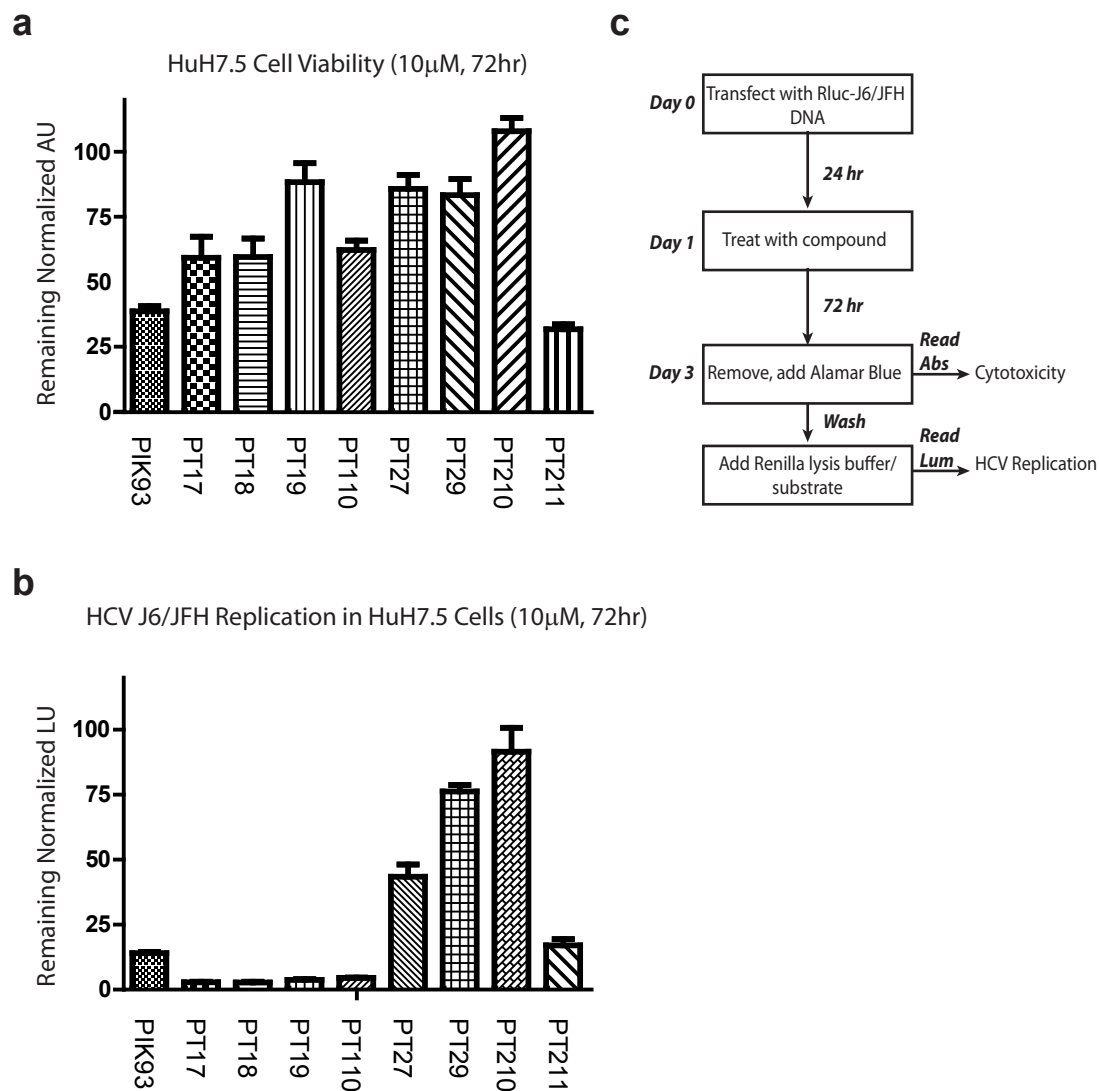


FIGURE 2. Cellular activity of selected phenylthiazole inhibitors in an HCV genotype 2a system. a, cytotoxicity of selected phenylthiazole inhibitors measured by alamar blue method. b, replication of J6/JFH measured by Renilla luciferase luminescence c, flowchart showing method for determining inhibition of HCV replication and cytotoxicity.

cyclopentanecarbonyl groups to PI4KIII β . Upon alignment of PI4KIII α with p110 γ (Introduction, Figure 3) it appears that the corresponding residue is G1763 or E1762, seemingly consistent with the small change in phenylthiazole IC₅₀ (3-fold) with bulky inhibitor substitution; the corresponding PI4KIII β residue appears to be E535 or K534, which would also be consistent with this theory. However, it should be noted that this alignment occurs in a region (P-loop, prior to beta-5) where similarity between PI4K and PI3K is low, making the assignment of these residues as analogous to W812 of p110 γ somewhat ambiguous.

Having identified inhibitors we predicted would be somewhat selective in cells, we next tested a subset of the inhibitors in an HCV genotype 2a¹³ luciferase reporter cell culture system for cytotoxicity and inhibition of HCV replication, in collaboration with Jeffrey Glenn and Michael Gelman at Stanford University (Figure 2). Here, we encountered our first caveat: although PIK93 appeared to inhibit HCV replication at 72 hours (~86%), a large part of that apparent inhibition was likely due to cell mortality, as cell viability was also inhibited significantly (~61%). A similar trend was observed for the other inhibitors—except for PT19 and PT110; in these cases replication was almost completely inhibited (~96%) while cell viability was relatively unaffected (88 and 62%, respectively). This implied to us that the bulkier trimethylacetyl and cyclopentanecarbonyl substitutions to the PIK93 scaffold were ablating binding to whatever off-targets might be damaging cell viability in the case of long-term PIK93 treatment.

Protein Kinase Inhibition of PIK93 and PT19

The minimal effect of PT19 on hepatocyte viability compared to PIK93 suggested that many toxic off-targets of PIK93 were eliminated by the bulkier *tert*-butyl substituent in PT19. Although we observed that affinity for PI3K was ablated by PT19-like modifications (Figure 1), we wondered whether protein kinase targets might account for the lessened toxicity of PT19. Accordingly, we submitted both PIK93 and PT19 for profiling with a panel of 313 protein kinases using Invitrogen's SelectScreen assay format (Figures 3 and 4). Overall, PIK93 at 1 micromolar concentration inhibited 35/313 kinases more than 40%. Most of the inhibited kinases were receptor tyrosine kinases (EPHA, ERBB, FLT, KIT, PDGFR family members); particularly potently inhibited were CDK8, DDR2, FLT3, MUSK, PDGFRA, and RET. Absent individual validation of targets, it is difficult to account for which protein kinase targets might contribute to cytotoxicity of PIK93; however, in every case, protein kinase targets inhibited by PIK93 were much less inhibited by a higher concentration of PT19 (10 micromolar). Moreover, in the case of the potently inhibited kinases, none were inhibited more than 40% by the higher concentration of PT19.

Elaboration of Phenylthiazole Inhibitors for Increased Potency

The identification of the PT19/PT110-like modifications which appear to drive selectivity versus protein and PI 3-kinases were encouraging; however, these compounds still had relatively low potency against HCV replication in hepatocytes (5-8 μ M). To discover more potent compounds, we decided to elaborate the sulfonamide position of PIK93, in the hope that there might be some difference in tolerance for various sulfonamide substituents of different bulk. The para-phenyl substituent was also modified in some cases, to explore a larger region of chemical space. Because the

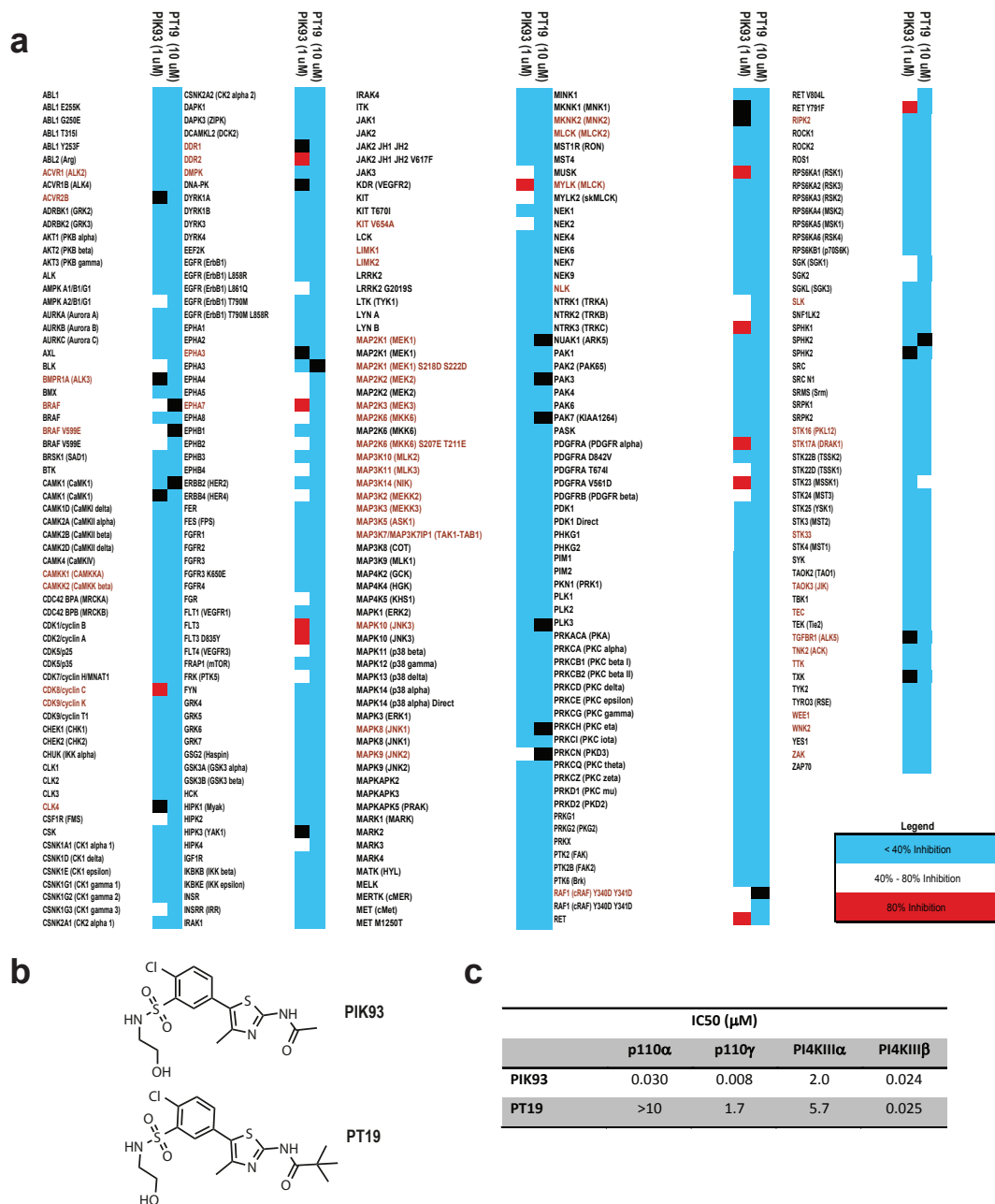


FIGURE 3. Summary of single-point inhibition of protein kinases by PIK93 and PT19. a, Invitrogen SelectScreen® results showing inhibition of a panel of protein kinases by PIK93 (1 μM) or PT19 (10 μM); blue signifies <40% inhibition, white signifies 40-80% inhibition, red signifies 80% inhibition or higher, and black signifies no data. b, structures of PIK93 and PT19; PT19 differs only in the replacement of the PIK93 acetamide with trimethylacetamide. c, biochemical IC50 values for PIK93 and PT19 against lipid kinases; PIK93 is >68-fold selective for PI4KIIIβ over PI3K p110γ/p110α.

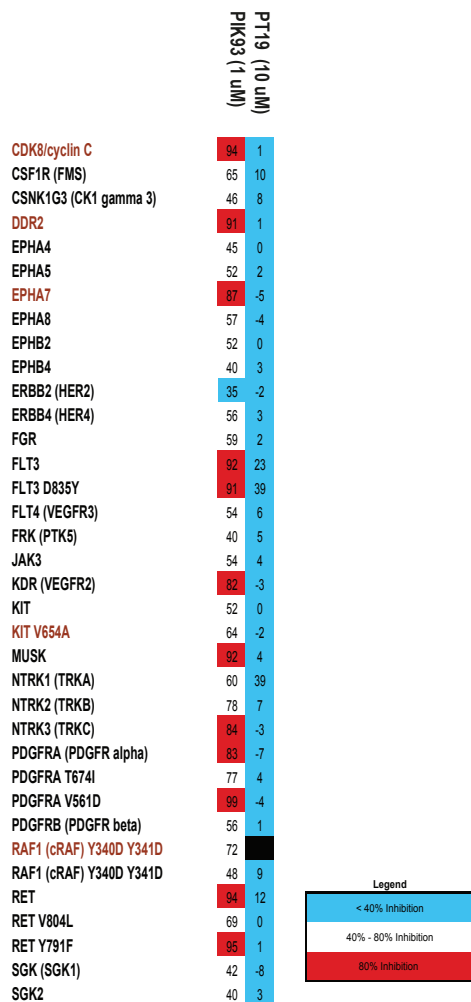


FIGURE 4. Change in inhibition of protein kinases by PIK93 and PT19. Same Invitrogen SelectScreen® results showing change in protein kinase inhibition between PIK93 and PT19; blue signifies <40% inhibition, white signifies 40-80% inhibition, red signifies 80% inhibition or higher, and black signifies no data; all protein kinase targets inhibited by PIK93 are no longer inhibited by the higher concentration of PT19.

synthetic method of figure 1 would have been overly laborious for these type of inhibitors, sulfonamide-substituted inhibitors were made by a slightly different method: the phenylthiazole core was first formed by Hantzsch cyclization between alpha-bromophenylketones and acylthiourea, and then the phenyl ring was derivatized by (long) treatment with chlorosulfonic acid and subsequent reaction with alkylamines. The resultant compounds were then assayed by Naveen Bojjireddy and Tamas Balla (NIH) against the same panel of kinases as in figure 1.

Unfortunately, every one of these derivatives (Figure 5) proved to be much worse against PI4Ks than the first round; none were less than 10 μ M against PI4K or less than 0.11 mM against PI4KIII β ; these compounds also showed poor activity against HCV replication in hepatocytes (data not shown). Both compounds with larger (PT47) and smaller (PT45) substituents in the sulfonamide position lost affinity for PI4Ks, indicating that perhaps there is some special feature of the PIK93 ethanolamino moiety. Intriguingly, none of these modifications had large effects on binding to PI3K p110 α or p110 γ ; for example, PT45 is as potent as PIK93 against and shows 80- and ~3000x selectivity versus PI4KIII β and PI4KIII α .

N-phenylsulfonamide Derivatives of PIK93

The fact that the ethanolamino moiety is tolerated in PIK93 despite the large effects due to substitution with other alkylamines suggested that the PI4Ks may have specific shape requirements in the vicinity of the sulfonamide binding area. Observing the structure of PIK93 bound to p110 γ (pdb code 2CHZ), we found that there appears to be enough steric allowance for substitution with an aniline in the sulfonamide position (Figure 6). Accordingly, we synthesized a panel of derivatives including phenyl, 4-

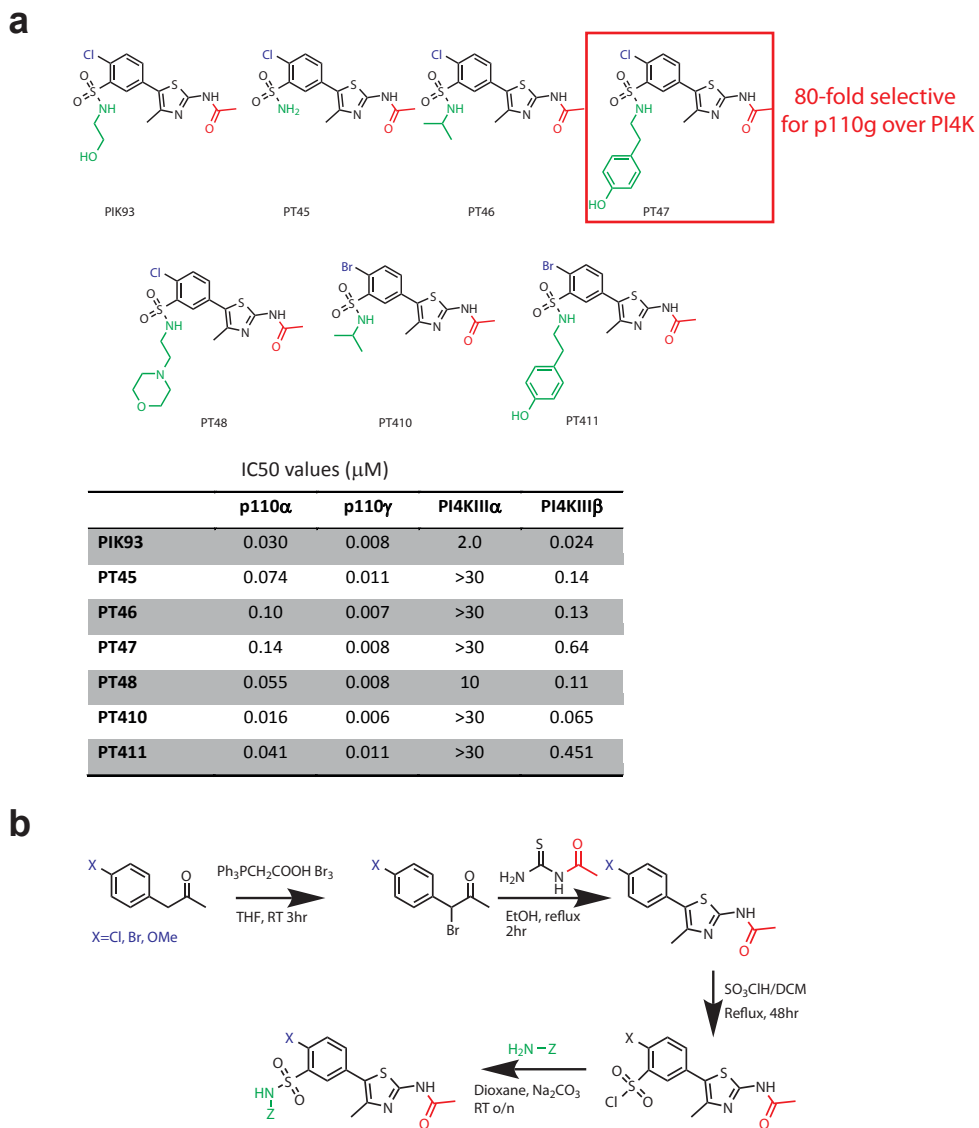


FIGURE 5. Effect of sulfonamide alkyl substitution on lipid kinase inhibition. a, structures of phenylthiazole inhibitors and IC₅₀ values against lipid kinases; replacement or ablation of the ethanolamino moiety of PIK93 causes large decreases in affinity for both PI4KIII α and PI4KIII β . b, IC₅₀ values (μM) against lipid kinases. c, synthetic scheme for phenylthiazole inhibitors.

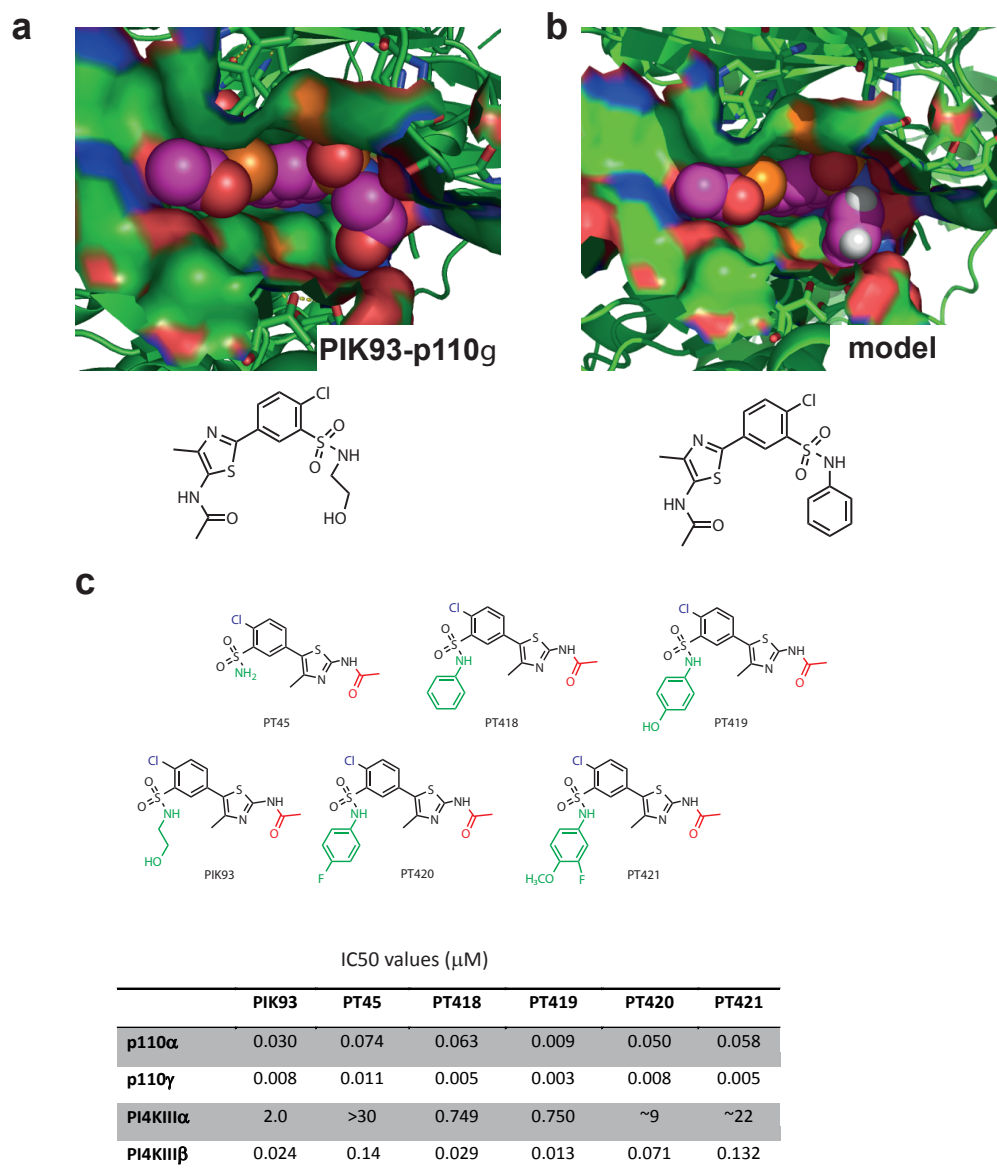
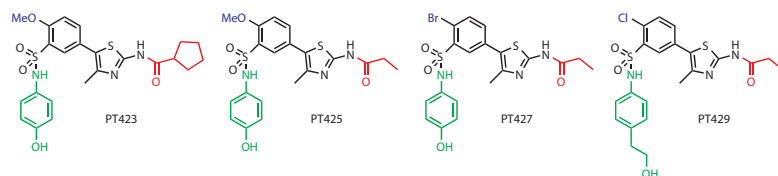


FIGURE 6. Effect of N-phenylsulfonamide derivatization on lipid kinase inhibition. a, binding site of p110 γ with PIK93 in sphere representation (pdb code 2CHZ). b, p110 γ binding site with aniline-derivatized PIK93 hand-docked; PIK93 binding pocket seems to be large enough to accommodate a phenyl substituent. c, structures and IC₅₀s for N-phenylsulfonamide derivatives and comparison compounds.

phenol, 4-fluorophenyl, and 4-methoxy,3-fluorophenyl groups according to the scheme in figure 5 and tested them against the standard panel of lipid kinases.

Although none of the compounds showed large increases in affinity for the PI4 kinases (Figure 6), this group of compounds was much better than the N-alkylsulfonamide derivatives; PT418 (phenyl) and PT419 (4-OH phenyl) show roughly comparable IC50s against PI4KIII α/β to PIK93. Interestingly, these values are much more potent than those for PT45 (the corresponding compound minus a phenyl ring), suggesting that a particular shape complementary interaction in the region where the PIK93 sulfonamide binds is necessary for PI4KIII α/β .

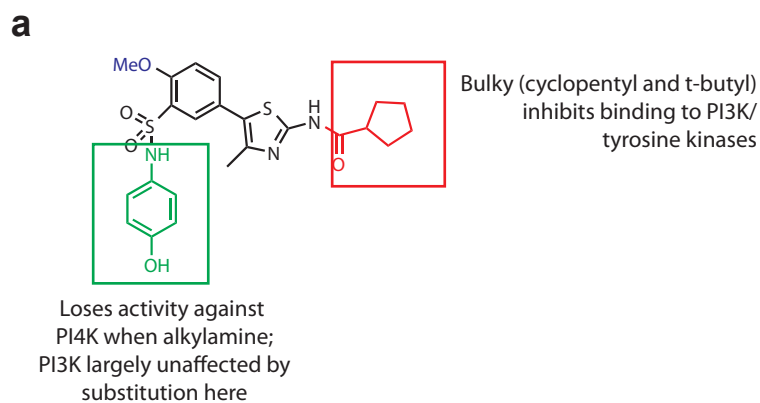
Despite the inability of N-phenylsulfonamide substitution to actually increase affinity for either PI4K isoform, we hypothesized that the feature could nonetheless be useful; the fact that it was roughly equivalent with the ethanolamino moiety of PIK93 seemed to imply that it would allow us to explore a different region of chemical space if combined with modifications to the acetamide and phenyl ring. To test this theory, we synthesized a small group of N-phenolsulfonamide inhibitors (Figure 7) possessing substitutions of the 4-chloride for 4-methoxide or 4-bromide and substitutions of the acetamide position for cyclopentanecarbonyl or propionyl. Much to our delight, these proved to be the most potent compounds for PI4Ks identified. PT423, 425, and 427 were all considerably more potent against PI4KIII β . than PIK93 (7/8/6nM vs 24 nM) and PT425 and PT427 showed improvements on PIK93 against PI4KIII α (0.511 and 0.292 vs 2.0 μ M). Curiously, none of the features of these inhibitors, when observed elsewhere in isolation, showed significant improvement against the PI4K enzymes, implying that this may be a combinatorial effect. Encouraged, we tested PT423/PT425/PT427 in cellular assays against HCV replication and observed dramatic



IC₅₀ values (μM)

	PT423	PT425	PT427	PT429
p110α	0.065	0.049	0.020	0.089
p110γ	0.064	0.078	0.010	0.006
PI4KIIIα	1.75	0.511	0.292	4.16
PI4KIIIβ	0.007*	0.008*	0.006*	0.026
HCV IC₅₀	0.365	0.800	0.434	1.7

FIGURE 7. Further derivatization of N-phenylsulfonamide inhibitors. *Value may approach limit of accurate detection for the IP kinase assay, where actual enzyme concentration is not known.



b

IC50 values (μM)

	PT19	PT110	PT423	PT425	PT427
p110α	>10	1.0	0.065	0.049	0.020
p110γ	1.7	0.56	0.064	0.078	0.010
PI4KIIIα	5.7	6.1	1.75	0.511	0.292
PI4KIIIβ	0.025	0.021	0.007*	0.008*	0.006*
HCV IC50	6.5	5.5	0.365	0.800	0.434
%Cell Survival (10 mM)	88.6	62.4	42.0	88.0	50.0

FIGURE 8. Summary of inhibitor development and SAR relationships gleaned from this survey. a, description of SAR relationships for PI4K, PI3K, and protein kinases. b, summary of most potent/selective compounds identified.

improvements against HCV replication compared to PT19/PT110; PT423 and PT427 were both active at less than 0.5 μM , much more potent than the 5-6 μM activity of PT19/PT110 (Figure 8b).

Final Issues: Decoupling of Off-targets and PI4KIII α/β Role in HCV Replication

Although we were able to identify inhibitors that exhibited significant improvements in activity against HCV replication and reduction of off-target cytotoxic effects, there remain some perplexing questions about the exact mechanism by which these inhibitors are functioning. Although we initially theorized that off-target activity was due to inhibition of PI3K and observed decreased cytotoxicity when PI3K activity was lowered, the data from the Invitrogen protein kinase screen indicates that these phenylthiazole derivatives of PIK93 probably have toxic off-targets other than lipid kinases—and that PI3K may not even be a toxic off-target, as PT423/425/427 show considerably potency against both PI3K isoforms and nonetheless have limited toxicity.

Moreover, the change in HCV potency of these compounds (~4-5x) relative to the PI4KIII β potency (the presumed relevant target for HCV replication here) (~10x) do not track perfectly with each other. It should be noted that the assay format for the PI4K enzymes involved using immunoprecipitated enzyme; and thus the true enzyme concentration in the assays is unknown—allowing the possibility that the compounds are actually more potent than they appear and that this fact is being unmasked in a cellular assay. Ultimately, the best way to resolve these issues will be to acquire further cellular data on direct effects of the inhibitors on PI(4)P production—correlation between HCV replication IC₅₀ and IC₅₀ for inhibition of PI(4)P production should shed light on the exact relationship between chemical inhibition of either PI4K isoform and HCV

replication. As dependence of HCV virus on host factors for replication is just beginning to be defined⁹, it is possible that HCV replication depends on activity of other phosphatidylinositol kinases; these experiments should shed light on that possibility.

Experimental Procedures

Assay of p110 α and p110 γ

p110 α -p85 complex and p110 γ were acquired from Millipore. Assays were performed with L α -phosphatidylinositol (Avanti) as described in Knight et al. Nat Protoc. 2007;2(10):2459-66. Inhibitor series were prepared 10% DMSO as 5x stocks for the assay.

Assays of HsVps34 were performed as described in Knight et al, except that the final assay buffer composition used was changed to 20mM HEPES 7.5, 100 mM NaCl, 3 mM MgCl, 1mg/mL PI and 44nM hvps34 was used in the assay. For inhibitors with an apparent IC₅₀ less than or equal to 22nM, values were reassayed using 4.4nM hvps34 with 3 mM MnCl₂.

Expression and Assay of PI4KIII α and PI4KIII β (Naveen Bojjireddy)

PI4KIII α and PI4KIII β assays were generously performed by Naveen Bojjireddy in the lab of Tamas Balla (NIH). COS-7 cells were cultured in 10 cm dishes and transfected at 70 % confluence with 10 μ g of plasmid DNA (HA-tagged bovine PI4KIII β , HA-tagged human PI4KIII α) using Lipofectamine 2000 and 5 ml Opti-MEM following the

manufacturers instructions. After 5 hours the transfection medium was replaced with 10 ml complete DMEM. 36 hrs post transfection, cells were washed once with 5 ml PBS (pH 7.4) and lysed in 1 ml of lysis buffer (1) on ice. Lysates were collected by scraping and after 15 min they were centrifuged at 13,000 rpm for 10 min. To the lysates was added 200 μ l of protein G Sepharose 4 fast flow beads that were prewashed with PBS and lysis buffer and 2 μ g of anti-HA antibody. The tubes were then incubated overnight at 4^oC in a tube rotator. The Sepharose beads in the lysate were washed twice with 150 mM NaCl in RIPA buffer, twice with RIPA buffer and once with kinase buffer (50 mM Tris/HCl, pH 7.5, 20 mM MgCl₂, 1 mM EGTA, 1 mM PtdIns, 0.4% Triton X-100, 0.5 mg/mL BSA) and finally the beads were resuspended in 200 μ L kinase buffer.

Kinase reactions were run in a mixture of 45 μ L of PI buffer (1 mM PI in kinase buffer), 10 μ L of immunoprecipitated beads, 2 μ L of inhibitors (dissolved and diluted in DMSO) or DMSO and 5 μ L of [γ -³²P]-ATP (1mM and 2 μ Ci/tube). The immunoprecipitates in PI buffer were pre-incubated with the drugs for 20 min prior the initiation of kinase reaction by adding ATP and the reactions were carried out for 30 min in 15 ml polypropolyne tubes. Reactions were terminated by addition of 3 ml of CHCl₃:CH₃OH:HCl (200:100:0.75) followed by 0.6 ml of 0.6N HCl to induce phase separation.. The mixtures were vortexed, centrifuged at 2000 rpm for 2 min and the upper phase was discarded. To the lower phase was added 1.5 ml of CHCl₃:CH₃OH:0.6N HCl (3:48:47) and the mixture vortexed and centrifuged at 2000 rpm for 2 min. The lower phase was then transferred to counting vials and evaporated. Samples were counted in a scintillation beta counter after adding 5 ml of Instafluor (Perkin-Elmer).

Assays for Cytotoxicity and HCV Replication (Michael Gelman)

Assays for cytotoxicity and HCV replication in HuH cells were generously performed by Michael Gelman (Stanford University). Huh7.5 cells were passaged according to usual cell culture procedures in DMEM + 10% FBS with the addition of nonessential amino acids, penicillin/streptomycin, and L-glutamine ("complete DMEM"). On day 0, the cells were trypsinized, washed twice with RNase-free PBS, and resuspended in RNase-free PBS (6×10^6 cells in 400 μ L). Genotype 2a HCV RNA (5 μ g, J6/JFH with a Renilla luciferase reporter) was added as a solution in <5 μ L RNase-free water, and the mixture was transferred to a 2mm electroporation cuvette. Electroporation was performed (5 pulses, 820 volts) and the cells were allowed to rest for 15 minutes, then diluted in complete DMEM to a final concentration of 2×10^5 cells/mL. The cells were plated into 96-well plates (100 μ L = 2×10^4 cells per well) and allowed to attach overnight.

On day 1, the media was removed and replaced with 200 μ L of complete DMEM containing 0.2% DMSO +/- varying concentrations of compound. The serial dilutions of compound were prepared in 1mL deepwell plates and transferred to culture plates in quadruplicate. The plates were then allowed to incubate for 3 days.

On day 4, media was again removed and the cells were washed with 100 μ L PBS, which was replaced with 10% alamarBlue in complete DMEM. The plates were incubated until a color differential was observable by eye between DMSO/DMEM control wells and negative control wells without cells. Plates were then read by a standard absorbance method on a Tecan M1000 plate reader. The cells were washed again with 100 μ L PBS, and then 30 μ L of Renilla assay lysis buffer (Promega) was added. The plates were placed on an orbital shaker at RT for 1 h, then frozen overnight at -80 C. Plates were thawed and read on a Tecan M1000 plate reader with luminometer using 10 μ L of 1X Renilla luciferase substrate (Promega). Data from the alamarBlue and luciferase assays

were normalized to 100% = no compound (DMSO vehicle), 0% = no cells. Analysis was performed in Excel 2008 (Microsoft) and Prism 5 (GraphPad).

General Methods—Compound Synthesis

Synthesis of 2-chloro-5-(2-oxopropyl)benzene-1-sulfonyl chloride (1)

3 mL 4-chlorophenylacetone (3.45g, 20.5 mmol) was added over 10 minutes dropwise to 15 mL (26.2g, 224 mmol) chlorosulfonic acid previously cooled to -20dC. The reaction was warmed to room temperature, then heated to 40dC for 2 hours. The reaction was then cooled to 4dC, quenched dropwise on 300 mL ice and extracted 3x with 100mL ethyl acetate. The organic layers were combined, washed with brine, and dried on sodium sulfate prior to reducing in vacuo to yield a brown oil (100%). The compound was used without further purification.

Synthesis of 2-chloro-N-(2-hydroxyethyl)-5-(2-oxopropyl)benzenesulfonamide (2)

Compound 1 (5.47g, 20.5 mmol) was dissolved in 30 mL dry THF and added dropwise to 4.5 mL ethanolamine (4.56g, 74.8 mmol) in 30 mL THF. The reaction was stirred at room temperature overnight and concentrated. The resultant concentrate was sonicated in 150 mL water and extracted 3x with ethyl acetate; the organic layers were combined, washed with brine, dried on sodium sulfate, and reduced in vacuo. The crude product was purified on 150g silica using a 2-10% gradient of methanol in dichloromethane, then by HPLC on a sorbax SB-C18 reverse phase column. Yield 0.53g (8.9%). ESI LC-ESI-MS: [MH]⁺ m/z calculated for C₁₁H₁₄ClNO₄S 292.03, found 292.14. ¹H NMR (400 MHz, DMSO) δ 7.76 (d, *J* = 2.1 Hz, 1H), 7.70 (t, *J* = 5.8 Hz, 1H), 7.56 (d, *J* = 8.1 Hz, 1H), 7.38 (dd, *J* = 8.1, 2.2 Hz, 1H), 3.91 (s, 2H), 3.34 (t, *J* = 6.5 Hz,

2H), 2.85 (dd, $J = 6.5, 6.0$ Hz, 2H), 2.14 (s, 3H). ^{13}C NMR (100 MHz, DMSO) δ 205.16, 137.56, 135.19, 134.85, 131.58, 131.38, 128.66, 59.83, 48.08, 44.89, 29.75.

Synthesis of 5-(1-bromo-2-oxopropyl)-2-chloro-N-(2-hydroxyethyl)benzenesulfonamide (3)

Compound 2 (0.205g, 0.70 mmol) dissolved in 10mL THF was added dropwise to a solution of 2-carboxyethyltriphenylphosphonium perbromide (Alfa) (0.434g, 0.753 mmol) in 5mL THF. The solution was stirred at room temperature for 1 hr or until decolorized. The reaction was filtered, concentrated in vacuo, and purified on silica in ethyl acetate to yield 0.189 g (72%). ESI LC-ESI-MS: $[\text{MH}]^+$ m/z calculated for $\text{C}_{11}\text{H}_{13}\text{BrClNO}_4\text{S}$ 368.94, found 369.2.

Synthesis of 2-methoxy-5-(2-oxopropyl)benzene-1-sulfonyl chloride (4)

4-methoxyphenylacetone (2 ml, 13 mmol) was added dropwise to 10 ml chlorosulfonic acid (17.5g, 149mmol) cooled to -20°C over 5 minutes. The reaction was allowed to stir for 30 minutes, warmed to room temperature and allowed to stir for 2 hours. The reaction was then cooled on ice and quenched by dropwise addition to 200 ml ice/water with stirring. Once the ice had melted, the reaction was extracted 3x with ethyl acetate, the organic layers were combined and washed with brine and sodium sulfate, and reduced in vacuo. The compound was taken to the next step without further purification (100%).

Synthesis of N-(2-hydroxyethyl)-2-methoxy-5-(2-oxopropyl)benzenesulfonamide (5)

Compound 4 was dissolved in 10 ml dry THF and added dropwise to a solution of 1.5 ml ethanolamine (1.52g, 28.3 mmol) in 10 ml THF. The reaction was allowed to

stir overnight and then reduced in vacuo. 50 ml water was added, and the aqueous layer was extracted 3x with ethyl acetate. The combined ethyl acetate was dried with brine and sodium sulfate, reduced in vacuo, and purified by flash chromatography in 0-10% methanol in dichloromethane. Yield 0.8 g (21%). LC-ESIMS [MH]⁺ m/z calculated for C₁₂H₁₇NO₅S, 288.08; found 287.94. ¹H NMR (400 MHz, DMSO) δ 7.54 (d, *J* = 2.2 Hz, 1H), 7.38 (dd, *J* = 8.5, 2.2 Hz, 1H), 7.16 (d, *J* = 8.5 Hz, 1H), 6.95 (t, *J* = 5.9 Hz, 1H), 4.63 (t, *J* = 5.6 Hz, 1H), 3.87 (s, 2H), 3.80 (s, 2H), 3.34 (dd, *J* = 12.0, 6.1 Hz, 3H), 2.78 (dd, *J* = 6.4 Hz, 2H), 2.13 (s, 3H). ¹³C NMR (100 MHz, DMSO) δ 205.83, 154.92, 135.53, 130.33, 127.40, 126.78, 112.68, 59.75, 56.16, 48.00, 45.11, 29.50.

Synthesis of 5-(1-bromo-2-oxopropyl)-N-(2-hydroxyethyl)-2-methoxybenzenesulfonamide (6)

5-(1-bromo-2-oxopropyl)-N-(2-hydroxyethyl)-2-methoxybenzenesulfonamide was synthesized by the method of compound 3 (75%). LC-ESIMS [MH]⁺ m/z calculated for C₁₂H₁₆BrNO₅S 365.99, found 365.73. ¹H NMR (400 MHz, DMSO) δ 7.82 (d, *J* = 2.4 Hz, 1H), 7.66 (dd, *J* = 8.7, 2.4 Hz, 1H), 7.27 (d, *J* = 8.7 Hz, 1H), 7.16 (t, *J* = 6.0 Hz, 1H), 3.92 (s, 4H), 3.35 (t, *J* = 6.5 Hz, 8H), 2.82 (q, *J* = 6.4 Hz, 3H), 2.28 (s, 3H). ¹³C NMR (100 MHz, DMSO) δ 199.08, 156.46, 135.13, 130.00, 128.11, 127.58, 113.30, 59.77, 56.39, 54.48, 45.06, 27.08.

Synthesis of N-carbamothioylpropionamide (acylthiourea 1)

To thiourea (1.0g, 13.1 mmol) in 40 mL dry toluene was added propionyl chloride (1.14 mL, 13.1 mmol) at room temperature. The reaction was heated to reflux for 16 hr, and the toluene was removed in vacuo. The concentrate was diluted in 200 mL ethyl acetate and washed 2x with water, once with brine, and dried on sodium sulfate. After concentration, the resulting solid was recrystallized from ethanol. Yield 0.5 g (29%). ¹H

NMR (400 MHz, DMSO) δ 11.03 (s, 1H), 9.64 (s, 1H), 9.33 (s, 1H), 2.36 (q, J = 7.5 Hz, 2H), 0.99 (t, J = 7.5 Hz, 3H). ^{13}C NMR (100 MHz, DMSO) δ 181.67, 174.58, 37.53, 17.76, 13.39.

Synthesis of N-carbamothioylbutyramide (acylthiourea 2)

N-carbamothioylbutyramide was prepared via the same procedure as acylthiourea 2. Yield 0.75g (39%). ^1H NMR (400 MHz, DMSO) δ 11.02 (s, 1H), 9.64 (s, 1H), 9.32 (s, 1H), 2.32 (t, J = 7.3 Hz, 2H), 1.51 (tq, J = 7.4 Hz, 1H), 0.85 (t, J = 7.4 Hz, 3H). ^{13}C NMR (100 MHz, DMSO) δ 181.67, 174.58, 37.53, 17.76, 13.39.

Synthesis of N-carbamothioylpivalamide (acylthiourea 3)

N-carbamothioylpivalamide was prepared via the same procedure as acylthiourea 2, omitting recrystallization and purifying on silica in 38% ethyl acetate in hexanes. Yield 0.26g (12%). ^1H NMR (400 MHz, DMSO) δ 10.27 (s, 1H), 9.74 (s, 1H), 9.39 (s, 1H), 1.19 (s, 1H). ^{13}C NMR (100 MHz, CD₃OD) δ 184.19, 180.79, 41.05, 26.91.

Synthesis of N-carbamothioylcyclopentanecarboxamide (acylthiourea 4)

N-carbamothioylcyclopentanecarboxamide was prepared by the same method as acylthiourea 3. Yield 1.37 g (61%). ^1H NMR (400 MHz, DMSO) δ 11.03 (s, 1H), 9.66 (s, 1H), 9.33 (s, 1H), 2.89 (ddt, J = 14.0, 8.5, 7.1 Hz, 1H), 1.90 – 1.74 (m, 2H), 1.70 – 1.57 (m, 4H), 1.56 – 1.42 (m, 2H). ^{13}C NMR (100 MHz, DMSO) δ 181.82, 177.77, 44.40, 29.77, 25.73.

Synthesis of N-carbamothioylcyclohexanecarboxamide (acylthiourea 5)

N-carbamothioylcyclohexanecarboxamide was prepared by the same method as acylthiourea 3. Yield 0.81g (33%). ^1H NMR (400 MHz, DMF) δ 11.04 (s, 1H), 9.90 (s,

1H), 9.28 (s, 1H), 2.61 (tt, $J = 11.5, 3.4$ Hz, 1H), 1.93 – 1.58 (m, 5H), 1.48 – 1.11 (m, 5H). ^{13}C NMR (100 MHz, DMSO) δ 181.98, 177.54, 43.77, 28.57, 25.17, 24.91.

Synthesis of PIK-93 (N-(5-(4-chloro-3-(N-(2-hydroxyethyl)sulfamoyl)phenyl)-4-methylthiazol-2-yl)acetamide)

Preparation of PIK-93 is described in Knight et al. Cell. 2006 May 19;125(4):733-47. ^1H NMR (400 MHz, DMSO) δ 12.21 (s, 1H), 7.94 (dd, 1H), 7.72 – 7.67 (m, 2H), 4.68 (t, 1H), 3.38 (dd, $J = 6.3$ Hz, 2H), 2.94 (dd, $J = 6.2$ Hz, 2H), 2.36 (s, 3H), 2.15 (s, 3H).

General Procedure for Synthesis of PT17-PT110 and PT27-PT211 (procedure A)

0.120 mmol of the corresponding bromoketone (4-Cl or 4-OMe) was combined with one equivalent of the corresponding thiourea (acylthioureas 1-5) in 5 ml dry ethanol and refluxed for 2 hours. The ethanol was removed in vacuo and the compounds were purified by C18 reverse phase chromatography, 5-95% acetonitrile in water with 0.1% TFA.

Synthesis of PT17 (N-(5-(4-chloro-3-(N-(2-hydroxyethyl)sulfamoyl)phenyl)-4-methylthiazol-2-yl)propionamide)

Yield 25%. ESI LC-ESI-MS: $[\text{MH}]^+$ m/z calculated for $\text{C}_{15}\text{H}_{18}\text{ClN}_3\text{O}_4\text{S}_2$, 404.04, found 404.5. ^1H NMR (400 MHz, DMSO) δ 7.96 (dd, $J = 1.9, 0.6$ Hz, 1H), 7.74 – 7.67 (m, 2H), 3.39 (dd, $J = 11.7, 6.3$ Hz, 2H), 2.95 (t, $J = 6.4$ Hz, 2H), 2.45 (q, $J = 7.5$ Hz, 2H), 2.37 (s, 3H), 1.10 (t, $J = 7.5$ Hz, 3H). ^{13}C NMR (100 MHz, DMSO) δ 172.25, 155.89, 143.70, 138.61, 133.00, 132.39, 131.72, 129.22, 128.93, 121.31, 59.94, 45.09, 28.23, 16.12, 9.12.

Synthesis of PT18 (N-(5-(4-chloro-3-(N-(2-hydroxyethyl)sulfamoyl)phenyl)-4-methylthiazol-2-yl)butyramide)

Yield 55%. ESI LC-ESI-MS: [MH]⁺ m/z calculated for C₁₆H₂₀CIN₃O₄S₂, 418.06, found 418.3. ¹H NMR (400 MHz, DMSO) δ 7.96 (dd, *J* = 1.7, 0.7 Hz, 1H), 7.74 – 7.65 (m, 2H), 3.39 (t, *J* = 6.4 Hz, 2H), 2.95 (t, *J* = 6.4 Hz, 2H), 2.41 (t, *J* = 7.3 Hz, 2H), 2.37 (s, 3H), 1.70 – 1.54 (m, 2H), 0.90 (t, *J* = 7.4 Hz, 3H). ¹³C NMR (100 MHz, DMSO) δ 171.45, 155.85, 143.70, 138.60, 133.00, 132.39, 131.73, 129.24, 128.94, 121.33, 59.94, 45.09, 36.79, 18.19, 16.11, 13.48.

Synthesis of PT19 (N-(5-(4-chloro-3-(N-(2-hydroxyethyl)sulfamoyl)phenyl)-4-methylthiazol-2-yl)pivalamide)

Yield 60%. ESI LC-ESI-MS: [MH]⁺ m/z calculated for C₁₇H₂₂CIN₃O₄S₂, 432.07, found 432.5. ¹H NMR (400 MHz, DMSO) δ 7.96 (d, *J* = 2.0 Hz, 1H), 7.75 – 7.66 (m, 2H), 3.40 (dd, *J* = 11.2, 6.0 Hz, 2H), 2.96 (t, *J* = 6.4 Hz, 2H), 2.39 (s, 3H), 1.24 (s, 9H). ¹³C NMR (100 MHz, DMSO) δ 176.92, 156.70, 143.60, 138.64, 133.01, 132.41, 131.78, 129.24, 128.93, 121.47, 59.95, 45.11, 38.80, 26.56, 16.01.

Synthesis of PT110 (N-(5-(4-chloro-3-(N-(2-hydroxyethyl)sulfamoyl)phenyl)-4-methylthiazol-2-yl)cyclopentanecarboxamide)

Yield 50%. ESI LC-ESI-MS: [MH]⁺ m/z calculated for C₁₈H₂₂CIN₃O₄S₂, 444.07, found 444.3. ¹H NMR (400 MHz, DMSO) δ 7.95 (dd, *J* = 1.9, 0.5 Hz, 1H), 7.74 – 7.66 (m, 2H), 3.39 (t, *J* = 6.4 Hz, 2H), 2.99 – 2.86 (m, *J* = 15.8, 6.9 Hz, 3H), 2.37 (s, 3H), 1.95 – 1.78 (m, 2H), 1.78 – 1.48 (m, 6H). ¹³C NMR (100 MHz, DMSO) δ 174.63, 156.07, 143.70, 138.62, 132.98, 132.40, 131.76, 129.23, 128.92, 121.36, 59.95, 45.10, 43.95, 29.89, 25.68, 16.11.

Synthesis of PT21 (N-(5-(3-(N-(2-hydroxyethyl)sulfamoyl)-4-methoxyphenyl)-4-methylthiazol-2-yl)acetamide)

Yield 53%. LC-ESI-MS [MH]⁺ m/z calcd for C₁₅H₁₉N₃O₅S₂, 386.08; found 385.94. ¹H NMR (400 MHz, DMSO) δ 7.72 (d, *J* = 2.3, 1H), 7.67 (dd, *J* = 8.5, 2.2, 1H), 7.30 (d, *J* = 8.7, 1H), 7.18 (s, 1H), 4.64 (s, 1H), 3.93 (s, 3H), 3.35 (dd, *J* = 12.3, 6.3, 2H), 2.85 (dd, *J* = 12.5, 6.3, 2H), 2.49 (m, DMSO), 2.31 (s, 3H), 2.13 (s, 3H).

Synthesis of PT27 (N-(5-(3-(N-(2-hydroxyethyl)sulfamoyl)-4-methoxyphenyl)-4-methylthiazol-2-yl)propionamide)

Yield 53%. ESI LC-ESI-MS: [MH]⁺ m/z calculated for C₁₆H₂₁N₃O₅S₂, 400.09 found ¹H NMR (400 MHz, DMSO) δ 7.73 (d, *J* = 2.4 Hz, 1H), 7.67 (dd, *J* = 8.6, 2.4 Hz, 1H), 7.31 (d, *J* = 8.7 Hz, 1H), 7.19 (t, *J* = 5.9 Hz, 1H), 3.94 (s, 3H), 3.35 (dt, *J* = 8.5, 5.0 Hz, 1H), 2.86 (dd, *J* = 12.5, 6.3 Hz, 2H), 2.43 (q, *J* = 7.5 Hz, 2H), 2.32 (s, 2H), 1.09 (t, *J* = 7.5 Hz, 3H). ¹³C NMR (100 MHz, DMSO) δ 172.02, 155.28, 155.00, 141.99, 134.09, 128.80, 128.31, 124.00, 122.18, 113.59, 59.81, 56.34, 45.15, 28.18, 15.79, 9.12.

Synthesis of PT29 (N-(5-(3-(N-(2-hydroxyethyl)sulfamoyl)-4-methoxyphenyl)-4-methylthiazol-2-yl)pivalamide)

Yield 85%. ESI LC-ESI-MS: [MH]⁺ m/z calculated for C₁₈H₂₅N₃O₅S₂, 428.12 found 428.3. ¹H NMR (400 MHz, DMSO) δ 11.81 (s, 1H), 7.73 (d, *J* = 2.4 Hz, 1H), 7.66 (dd, *J* = 8.6, 2.4 Hz, 1H), 7.31 (d, *J* = 8.7 Hz, 1H), 7.19 (t, *J* = 5.9 Hz, 1H), 3.93 (s, 3H), 3.37 (t, *J* = 6.4 Hz, 2H), 2.86 (dd, *J* = 6.3 Hz, 2H), 2.33 (s, 3H), 1.23 (s, 9H).

Synthesis of PT210 (N-(5-(3-(N-(2-hydroxyethyl)sulfamoyl)-4-methoxyphenyl)-4-methylthiazol-2-yl)cyclopentanecarboxamide)

Yield 73%. ESI LC-ESI-MS: [MH]⁺ m/z calculated for C₁₉H₂₅N₃O₅S₂, 440.12 found 440.6. ¹H NMR (400 MHz, DMSO) δ 12.10 (s, 1H), 7.72 (d, *J* = 2.4 Hz, 1H), 7.66 (dd, *J* = 8.6, 2.4 Hz, 1H), 7.31 (d, *J* = 8.7 Hz, 1H), 7.19 (t, *J* = 5.9 Hz, 1H), 3.93 (s, 3H),

3.41 – 3.30 (m, 3H), 2.85 (dd, 1H), 2.31 (s, 3H), 1.87 (dd, $J = 13.3, 6.2$ Hz, 2H), 1.75 – 1.45 (m, 6H).

Synthesis of PT211 (N-(5-(3-(N-(2-hydroxyethyl)sulfamoyl)-4-methoxyphenyl)-4-methylthiazol-2-yl)cyclohexanecarboxamide)

Yield 61%. ESI LC-ESI-MS: $[MH]^+$ m/z calculated for $C_{20}H_{27}N_3O_5S_2$, 454.14, found 454.4. 1H NMR (400 MHz, DMSO) δ 7.72 (d, $J = 2.4$ Hz, 1H), 7.66 (dd, $J = 8.6, 2.4$ Hz, 1H), 7.30 (d, $J = 8.7$ Hz, 1H), 3.93 (s, 3H), 3.39 – 3.31 (m, 2H), 2.88 – 2.82 (m, 2H), 2.31 (s, 2H), 1.85 – 1.66 (m, 4H), 1.63 (d, $J = 10.1$ Hz, 1H), 1.39 (dd, $J = 24.1, 12.2$ Hz, 2H), 1.31 – 1.11 (m, 4H).

General Procedure for Synthesis of Un-sulfonylated Phenylthiazoles (procedure B)

11.6 mmol (0.97equiv) of 2-carboxyethyltriphenylphosphonium perbromide (Alfa) was dissolved in 50 mL dry THF in a flame-dried flask. 12 mmol (1 equiv) of the corresponding phenylacetone derivative (4-Cl, 4-OMe, or 4-Br) was added dropwise under high stirring. A catalytic amount of benzoyl peroxide was added, and the reaction was allowed to stir until precipitation was complete and reaction was decolorized (approx 1-2hr). The reaction was filtered, THF removed in vacuo, and the residue was resuspended in dry ethanol. N-acetylthiourea (Acros) (1 equiv, 12 mmol) was added and the reaction was refluxed for 30m. The ethanol was then removed in vacuo and the residue was purified on silica in 1% methanol in dichloromethane.

Synthesis of N-(5-(4-bromophenyl)-4-methylthiazol-2-yl)acetamide

Yield 45%. ESI LC-ESI-MS: $[MH]^+$ m/z calculated for $C_{12}H_{11}BrN_2OS$ 310.98, found 311.2. 1H NMR (400 MHz, DMSO) δ 12.14 (s, 1H), 7.67 – 7.58 (m, 2H), 7.44 –

7.36 (m, 2H), 2.33 (s, 3H), 2.14 (s, 3H). ¹³C NMR (100 MHz, DMSO) δ 168.39, 155.37, 142.56, 131.78, 131.44, 130.41, 122.58, 120.29, 22.42, 16.02.

Synthesis of N-(5-(4-chlorophenyl)-4-methylthiazol-2-yl)acetamide

Yield 63%. ESI LC-ESI-MS: [MH]⁺ m/z calculated for C₁₂H₁₁CIN₂OS 267.03. found 267.17. ¹H NMR (400 MHz, DMSO) δ 12.13 (s, 1H), 7.51 – 7.44 (m, 4H), 2.33 (s, 3H), 2.14 (s, 3H). ¹³C NMR (100 MHz, DMSO) δ 168.38, 155.35, 142.53, 131.78, 131.07, 130.14, 128.87, 122.55, 22.42, 16.00.

Synthesis of N-(5-(4-methoxyphenyl)-4-methylthiazol-2-yl)acetamide

Yield 74%. ESI LC-ESI-MS: [MH]⁺ m/z calculated for C₁₃H₁₄N₂O₂S 263.08, found 263.21. ¹H NMR (400 MHz, DMSO) δ 12.03 (s, 1H), 7.39 – 7.33 (m, 1H), 7.03 – 6.97 (m, 1H), 3.78 (s, 1H), 2.30 (s, 1H), 2.13 (s, 3H). ¹³C NMR (100 MHz, DMSO) δ 168.16, 158.47, 154.51, 140.95, 129.82, 124.24, 123.73, 114.34, 55.18, 22.42, 15.82.

General Procedure for Synthesis of PT 45, PT46, PT47, PT48, PT410, PT411, PT418-PT421 (procedure C)

The corresponding phenylthiazoles (4-Cl, 4-Br) were chlorosulfonated by adding them dropwise as a 0.25M suspension in dichloromethane to an excess (106 equiv) chlorosulfonic acid at -20dC. The reaction was refluxed for 48 hours (4-halogen) at 40dC or stirred at RT for 24 hours (4-methoxy) under argon. Yields of 4-halogenated phenylthiazoles were enhanced by longer reaction times. The reaction was quenched dropwise on ice, extracted 3x with dichloromethane, and the dichloromethane layers were combined, washed with brine, dried on sodium sulfate and concentrated to generate the sulfonyl chlorides of the phenylthiazoles. 0.66 mmol of each sulfonyl chloride was then combined in 5mL dioxane with 2 equivalents of sodium carbonate

(supplied as a 2M solution) and 2 equivalents of the corresponding amine and stirred overnight. The dioxane was then removed in vacuo, the residue brought up in 200 mL water, and extracted 4x with ethyl acetate. The ethyl acetate layers were then combined and concentrated in vacuo to yield the crude sulfonated phenylthiazoles, which were purified on C18 reverse phase, 5-95% acetonitrile in water, 0.1% TFA.

Synthesis of PT45 (N-(5-(4-chloro-3-sulfamoylphenyl)-4-methylthiazol-2-yl)acetamide)

Ammonia was supplied as a saturated solution in water, and 20 equivalents were added. Yield 15%. ESI LC-ESI-MS: [MH]⁺ m/z calculated for C₁₂H₁₂ClN₃O₃S₂ 346.0, found 346.5.

Synthesis of PT46 (N-(5-(4-chloro-3-(N-isopropylsulfamoyl)phenyl)-4-methylthiazol-2-yl)acetamide)

13% yield. ESI LC-ESI-MS: [MH]⁺ m/z calculated for C₁₅H₁₈ClN₃O₃S₂ 388.05, found 388.4. ¹H NMR (400 MHz, DMSO) δ 12.22 (s, 1H), 7.97 (t, *J* = 1.3 Hz, 1H), 7.92 (d, *J* = 8.0 Hz, 1H), 7.70 (d, *J* = 1.2 Hz, 1H), 3.48 – 3.23 (m, *J* = 13.3, 6.8 Hz, 1H), 2.36 (s, 3H), 2.15 (s, 3H), 1.01 (d, *J* = 6.6 Hz, 6H).

Synthesis of PT47 (N-(5-(4-chloro-3-(N-(4-hydroxyphenethyl)sulfamoyl)phenyl)-4-methylthiazol-2-yl)acetamide)

9.3% yield. ESI LC-ESI-MS: [MH]⁺ m/z calculated for C₂₀H₂₀ClN₃O₄S₂ 466.06, found 466.7. ¹H NMR (400 MHz, DMSO) δ 12.22 (s, 1H), 8.03 (t, *J* = 5.7 Hz, 1H), 7.93 (dd, *J* = 1.9, 0.6 Hz, 1H), 7.71 – 7.64 (m, 2H), 7.06 – 6.81 (m, 2H), 6.69 – 6.53 (m, 2H), 3.07 (dd, *J* = 14.5, 6.2 Hz, 1H), 2.64 – 2.54 (m, 2H), 2.36 (s, 3H), 2.16 (s, 3H).

Synthesis of PT48 (N-(5-(4-chloro-3-(N-(2-morpholinoethyl)sulfamoyl)phenyl)-4-methylthiazol-2-yl)acetamide)

6% yield. ESI LC-ESI-MS: [MH]⁺ m/z calculated for C₁₈H₂₃ClN₄O₄S₂ 459.08, found 459.6.

Synthesis of PT410 (N-(5-(4-bromo-3-(N-isopropylsulfamoyl)phenyl)-4-methylthiazol-2-yl)acetamide)

5% yield. ESI LC-ESI-MS: [MH]⁺ m/z calculated for C₁₅H₁₈BrN₃O₃S₂ 432.00, found 432.5.

Synthesis of PT411 (N-(5-(4-bromo-3-(N-(4-hydroxyphenethyl)sulfamoyl)phenyl)-4-methylthiazol-2-yl)acetamide)

14% yield. ESI LC-ESI-MS: [MH]⁺ m/z calculated for C₂₀H₂₀BrN₃O₄S₂ 510.01, found 510.5.

Synthesis of PT418 (N-(5-(4-chloro-3-(N-phenylsulfamoyl)phenyl)-4-methylthiazol-2-yl)acetamide)

33% yield. ESI LC-ESI-MS: [MH]⁺ m/z calculated for C₁₈H₁₆ClN₃O₃S₂ 422.03, found 422.2.

Synthesis of PT419 (N-(5-(4-chloro-3-(N-(4-hydroxyphenyl)sulfamoyl)phenyl)-4-methylthiazol-2-yl)acetamide)

16% yield. ESI LC-ESI-MS: [MH]⁺ m/z calculated for C₁₈H₁₆ClN₃O₄S₂, 438.03 found 438.17.

Synthesis of PT420 (N-(5-(4-chloro-3-(N-(4-fluorophenyl)sulfamoyl)phenyl)-4-methylthiazol-2-yl)acetamide)

55% yield. ESI LC-ESI-MS: [MH]⁺ m/z calculated for C₁₈H₁₅ClFN₃O₃S₂ 440.02, found 440.16.

Synthesis of PT421 (N-(5-(4-chloro-3-(N-(3-fluoro-4-methoxyphenyl)sulfamoyl)phenyl)-4-methylthiazol-2-yl)acetamide)

41% yield. ESI LC-ESI-MS: [MH]⁺ m/z calculated for C₁₉H₁₇ClFN₃O₄S₂ 470.03, found 470.14.

Synthesis of 5-(4-methoxyphenyl)-4-methylthiazol-2-amine

N-(5-(4-methoxyphenyl)-4-methylthiazol-2-yl)acetamide (0.4g, 1.52 mmol) was dissolved in 33% EtOH containing 10% aqueous HCl. The solution was refluxed for 4 hours and poured on 150mL water. The pH was adjusted to 12, the aqueous layer was extracted 4x with ethyl acetate, and the ethyl acetate layers were washed with brine and magnesium sulfate and concentrated to yield the free amine (74%). ESI LC-ESI-MS: [MH]⁺ m/z calculated for C₁₁H₁₂N₂O₂S 221.07, found 220.89.

Synthesis of N-(5-(4-methoxyphenyl)-4-methylthiazol-2-yl)cyclopentanecarboxamide

5-(4-methoxyphenyl)-4-methylthiazol-2-amine (0.22 mmol) was dissolved in 0.5 mL dry pyridine and treated with 0.44 mmol cyclopentanecarbonyl chloride. The reaction was stirred until precipitation completed, and then the reaction was diluted to 20mL with water. The water was washed 3x with ethyl acetate, and the ethyl acetate layers were combined and washed 2x with 10% CuSO₄. The organics were then washed 3x with saturated bicarbonate, dried on magnesium sulfate, and concentrated to yield the carboxamide (50%). ESI LC-ESI-MS: [MH]⁺ m/z calculated for C₁₇H₂₀N₂O₂S 317.12, found 316.93.

Synthesis of PT423 (N-(5-(3-(N-(4-hydroxyphenyl)sulfamoyl)-4-methoxyphenyl)-4-methylthiazol-2-yl)cyclopentanecarboxamide)

PT423 was synthesized by procedure C, using N-(5-(4-methoxyphenyl)-4-methylthiazol-2-yl)cyclopentanecarboxamide as the phenylthiazole for chlorosulfonation (17% yield). ESI LC-ESI-MS: [MH]⁺ m/z calculated for C₂₃H₂₅N₃O₅S₂ 488.12, found 488.28.

Synthesis of N-(5-(4-methoxyphenyl)-4-methylthiazol-2-yl)propionamide

N-(5-(4-methoxyphenyl)-4-methylthiazol-2-yl)propionamide was synthesized by the method of N-(5-(4-methoxyphenyl)-4-methylthiazol-2-yl)cyclopentanecarboxamide (40% yield). ESI LC-ESI-MS: [MH]⁺ m/z calculated for C₁₄H₁₆N₂O₂S 277.09, found 277.20.

Synthesis of PT425 (N-(5-(3-(N-(4-hydroxyphenyl)sulfamoyl)-4-methoxyphenyl)-4-methylthiazol-2-yl)propionamide)

PT425 was synthesized by procedure C, using N-(5-(4-methoxyphenyl)-4-methylthiazol-2-yl)propionamide as the substrate for chlorosulfonation (17% yield). ESI LC-ESI-MS: [MH]⁺ m/z calculated for C₂₀H₂₁N₃O₅S₂ 448.09, found 448.24.

Synthesis of 5-(4-bromophenyl)-4-methylthiazol-2-amine

5-(4-bromophenyl)-4-methylthiazol-2-amine was produced by the method of 5-(4-methoxyphenyl)-4-methylthiazol-2-amine (78%). ESI LC-ESI-MS: [MH]⁺ m/z calculated for C₁₀H₉BrN₂S 268.97, found 269.12.

Synthesis of N-(5-(4-bromophenyl)-4-methylthiazol-2-yl)propionamide

N-(5-(4-bromophenyl)-4-methylthiazol-2-yl)propionamide was synthesized by the method of N-(5-(4-methoxyphenyl)-4-methylthiazol-2-yl)propionamide (78%). ESI LC-ESI-MS: [MH]⁺ m/z calculated for C₁₃H₁₃BrN₂OS 324.99, found 325.11.

Synthesis of PT427 (N-(5-(4-bromo-3-(N-(4-hydroxyphenyl)sulfamoyl)phenyl)-4-methylthiazol-2-yl)propionamide)

PT427 was synthesized by the method of PT425 (18% yield). ESI LC-ESI-MS: [MH]⁺ m/z calculated for C₁₉H₁₈BrN₃O₄S₂ 495.99, found 496.07.

Synthesis of 5-(4-chlorophenyl)-4-methylthiazol-2-amine

5-(4-chlorophenyl)-4-methylthiazol-2-amine was produced by the method of 5-(4-methoxyphenyl)-4-methylthiazol-2-amine (80%). ESI LC-ESI-MS: [MH]⁺ m/z calculated for C₁₀H₉ClN₂S 225.02, found 225.13.

Synthesis of N-(5-(4-chlorophenyl)-4-methylthiazol-2-yl)propionamide

N-(5-(4-chlorophenyl)-4-methylthiazol-2-yl)propionamide was synthesized by the method of N-(5-(4-methoxyphenyl)-4-methylthiazol-2-yl)propionamide (70%). ESI LC-ESI-MS: [MH]⁺ m/z calculated for C₁₃H₁₃ClN₂OS 281.14, found 281.22.

Synthesis of PT429 (N-(5-(4-chloro-3-(N-(4-(2-hydroxyethyl)phenyl)sulfamoyl)phenyl)-4-methylthiazol-2-yl)propionamide)

PT429 was synthesized by the method of PT423 (22%). ESI LC-ESI-MS: [MH]⁺ m/z calculated for C₂₁H₂₂ClN₃O₄S₂ 480.07, found 480.21.

References

1. Marone, R. et al. Targeting phosphoinositide 3-kinase: moving towards therapy. *Biochimica et biophysica acta* **1784**, 159-85(2008).
2. Clamp, M. et al. The Jalview Java alignment editor. *Bioinformatics (Oxford, England)* **20**, 426-7(2004).
3. Audhya, a, Foti, M. & Emr, S.D. Distinct roles for the yeast phosphatidylinositol 4-kinases, Stt4p and Pik1p, in secretion, cell growth, and organelle membrane dynamics. *Molecular biology of the cell* **11**, 2673-89(2000).
4. Balla, A. et al. Maintenance of hormone-sensitive phosphoinositide pools in the plasma membrane requires phosphatidylinositol 4-kinase IIIalpha. *Molecular biology of the cell* **19**, 711-21(2008).
5. Bruns, J.R. et al. Multiple roles for phosphatidylinositol 4-kinase in biosynthetic transport in polarized Madin-Darby canine kidney cells. *The Journal of biological chemistry* **277**, 2012-8(2002).
6. Tóth, B. et al. Phosphatidylinositol 4-kinase IIIbeta regulates the transport of ceramide between the endoplasmic reticulum and Golgi. *The Journal of biological chemistry* **281**, 36369-77(2006).

7. De Matteis, M.A., Di Campli, A. & Godi, A. The role of the phosphoinositides at the Golgi complex. *Biochimica et biophysica acta* **1744**, 396-405(2005).
8. Borawski, J. et al. Class III phosphatidylinositol 4-kinase alpha and beta are novel host factor regulators of hepatitis C virus replication. *Journal of virology* **83**, 10058-74(2009).
9. Tai, A.W. et al. A functional genomic screen identifies cellular cofactors of hepatitis C virus replication. *Cell host & microbe* **5**, 298-307(2009).
10. Hsu, N.-Y. et al. Viral reorganization of the secretory pathway generates distinct organelles for RNA replication. *Cell* **141**, 799-811(2010).
11. Knight, Z. a et al. A pharmacological map of the PI3-K family defines a role for p110alpha in insulin signaling. *Cell* **125**, 733-47(2006).
12. Miller, S. et al. Shaping development of autophagy inhibitors with the structure of the lipid kinase Vps34. *Science (New York, N. Y.)* **327**, 1638-42(2010).
13. Lindenbach, B.D. et al. Complete replication of hepatitis C virus in cell culture. *Science (New York, N. Y.)* **309**, 623-6(2005).

CHAPTER 3: NEW SIGNALING ROLES FOR HUMAN CARBONYL REDUCTASE I REVEALED BY ENZYMOLOGY

The Short-Chain Dehydrogenase Family and CBR1

Carbonyl Reductase I belongs to the SDR family of short chain NAD(P)H-dependent dehydrogenases/reductases that comprise a relatively large family of approximately 140 enzymes in humans. While all members of the SDR family utilize nicotinamide cofactor to perform reductive or oxidative reactions on small molecules, exhibit the Rossman fold characteristic of dinucleotide cofactor binding enzymes, and require a central catalytic tyrosine residue, SDRs are highly structurally variable and typically have low sequence homology, presumably because of early evolutionary divergence¹. Consistent with this wide diversity in structure, SDRs are known to act on a very large selection of substrates unrelated except for redox-labile functionalities; examples of substrates include steroids, eicosanoids, xenobiotic compounds, and aliphatic reactive electrophiles

The diversity for substrates acted on by members of the SDR family reflects the diversity of functions for metabolism of carbonyl/hydroxy groups (the largest chemical group acted upon by SDRs) in cellular biochemistry. Reduction of a carbonyl group on a ligand can activate binding to a cellular receptor (as in the keto groups of steroids), provide a conjugation site for conversion into more easily excreted glucuronidated or sulfated forms (in the case of highly lipophilic molecules), or ablate toxicity due to promiscuous cellular reactivity (as in the case of radical-generating quinones and thiol/amine reactive aldehydes). Thus SDRs that act on carbonyl groups would seem to play an analogous (phase I metabolism) but orthogonal biological role to cytochrome-

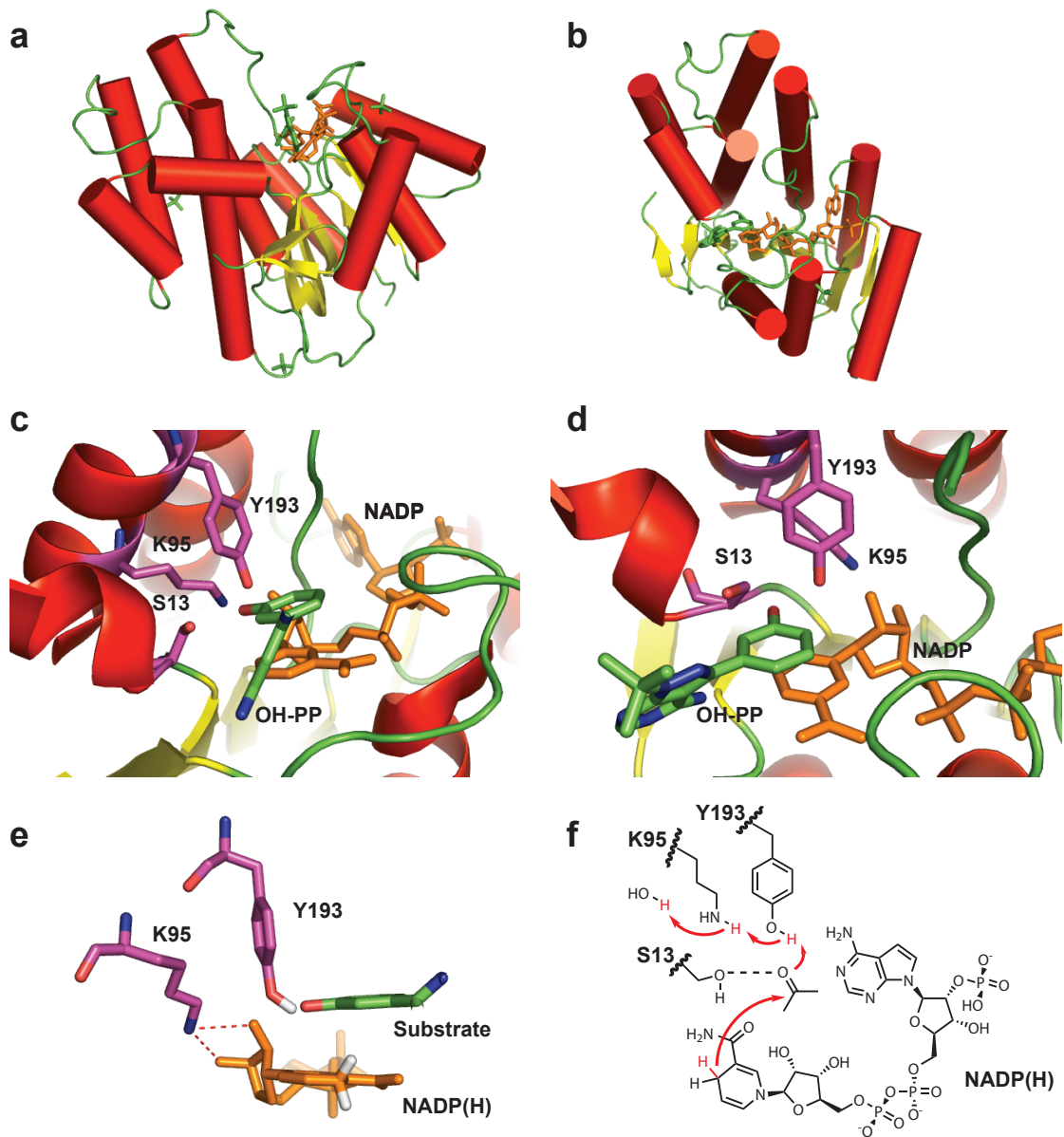


FIGURE 1. Fold and structural features of CBR1-OH-PP-NADP (PDB code 1WMA). *a* and *b*, cylinder representations showing the Rossman fold of CBR1; alpha helices (red) flank and inner core of beta sheets (yellow), NADP (orange) and the substrate-mimetic OH-PP (green) bind in the cleft formed between two groups of alpha helices. *c* and *d*, cartoon and stick representation of CBR1 binding site; catalytic triad consisting of Y293, K95, and S13 are highlighted. *e* and *f*, proposed model of carbonyl reduction by CBR1; Y193 acts as a general acid, donating a proton to the substrate oxygen upon hydride transfer from nicotinamide, S13 acts to polarize the oxygen-carbon bond, and K95 provides a proton relay and stabilizes cofactor conformation.

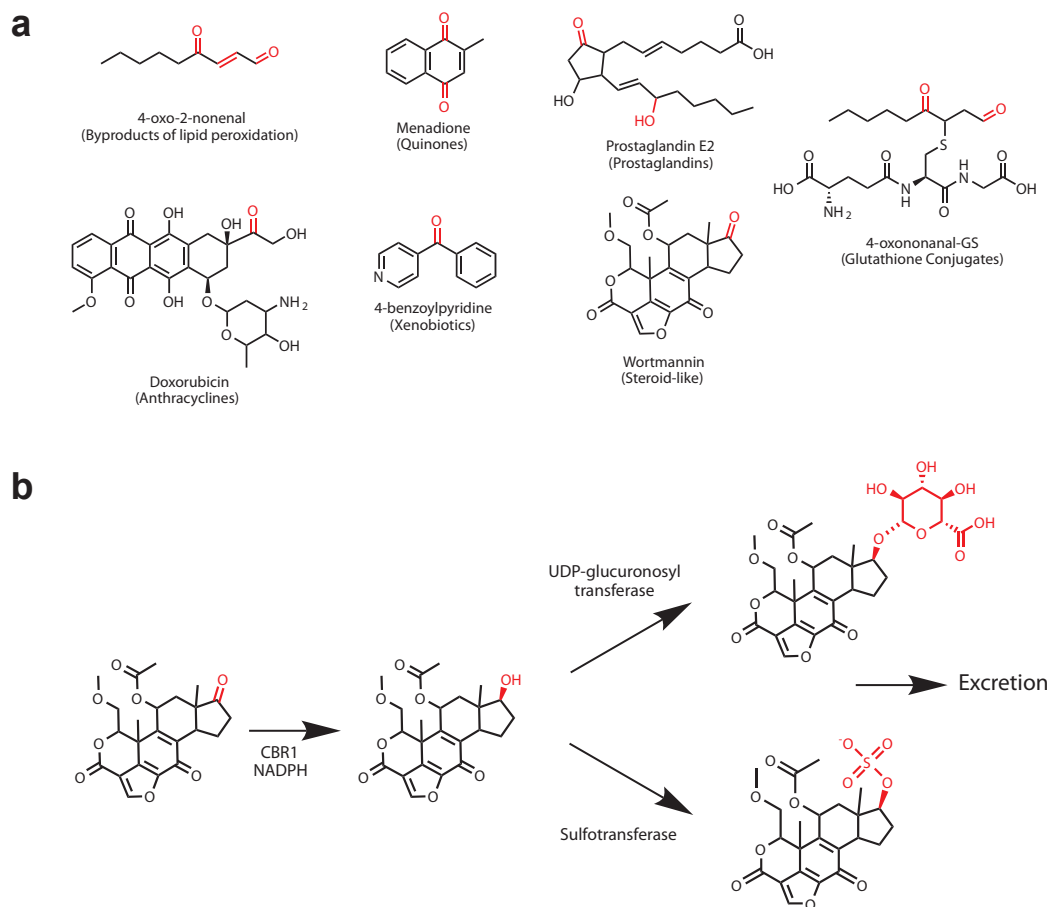


FIGURE 2. Diversity and function of CBR1 reduction. *a*, selection of substrates reported in the literature to be reduced by CBR1; functional groups known to be reduced are highlighted in red. Note the absence of consistent structural determinants of activity. *b*, proposed mechanism by which carbonyl reduction by CBR1 (phase I metabolism) can unmask carbonyl groups as substrates for phase II conjugation reactions and eventual detoxification/excretion; wortmannin is reduced in the 17-keto position by CBR1 and the resultant 17-OH can serve as a substrate for UDP-glucuronosyl transferases or sulfotransferases, generating a more water-soluble metabolite too sterically hindered to bind its target.

P450 enzymes, which facilitate many of the same processes but via oxygen insertion² rather than carbonyl formation/reduction.

While many SDRs exhibit exquisite selectivity for a single substrate and tissue-specific localization, suggesting involvement primarily in signaling processes by endogenous hormones (e.g. 11 β -hydroxysteroid dehydrogenase 1, which converts cortisone to the active glucocorticoid agonist cortisol³), more stereotypical is the CBR1-type mode of promiscuous activity for a large diversity of carbonyl-containing substrates (Figure 1b). Previous studies have demonstrated the ability of CBR1 to act on carbonyl groups that span the substrate spectrum for SDR enzymes—from prostaglandin E2 and quinones like menadione⁴ to toxic cellular byproducts like 4-oxo-2-nonenal⁵ to microbial toxins like daunorubicin⁶ and wortmannin⁷. In general, action by CBR1 converts the substrates to forms that have lower toxicity/reactivity or are more easily eliminated from the body (e.g. hydroquinones from quinones). This data point, combined with the ubiquitous expression of CBR1⁸ (although elevated levels are observed in the CNS, liver, and lung), suggests that the primary cellular role of CBR1 is small-molecule detoxification.

hCBR1 and GSNO Reduction--Enzymology

CBR1 has been previously demonstrated to possess a glutathione binding site and to bind glutathione adducts of small molecules⁹. In an attempt to understand the selectivity of CBR1 for glutathione conjugates, CBR1 was serendipitously discovered to facilitate reduction of S-nitrosoglutathione (GSNO) in a NADPH-dependent manner. As GSNO is believed to be a critical mediator of nitric oxide signaling in cells¹⁰, we sought to

validate whether or not this new activity of CBR1 could represent a new physiological role for CBR1.

The relevant group for GSNO reduction is a –SNO group, whereas CBR1 has previously only been shown to act on carbonyl groups; hence, there was a strong possibility that reduction of GSNO by CBR1 represented a low-efficiency process that might not represent a significant amount of CBR1 activity in cells. To discount this possibility, the kinetic constants for reduction of hCBR1 (K_M and k_{cat}) were determined at saturating concentrations of NADPH to compare the efficiency of GSNO reduction relative to established substrates of CBR1. Confirming the biochemical relevance of GSNO reduction by CBR1, both K_M and k_{cat} (30.1 μM and 450 min^{-1}) were shown to be comparable to that of CBR1 for its prototypical substrate menadione (22 μM and 402 min^{-1})¹¹. Thus, although CBR1 does not turn over GSNO as efficiently as the other reported GSNO reductase (hFDH, k_{cat} =2400 min^{-1}), GSNO is bound and turned over by CBR1 at least as well as its other substrates. However, the cofactor specificity of hCBR1 (NADPH rather than NADH) suggests that hCBR1 GSNO reduction may be more physiologically significant as previous studies have shown that NADP(H) exists primarily in the reduced state while NAD(H) exists primarily in the oxidized state^{12,13} (making NADP(H) the “reductive” cofactor and NAD(H) the “oxidative” one).

The consistency of k_{cat} between GSNO and other CBR1 substrates indicated that, at least in the case of GSNO, CBR1 acts as efficiently on –SNO groups as on carbonyl groups; however, this raised the question of exactly which functional group transformation was being performed on GSNO. To shed light on this transformation, we first determined the stoichiometry of GSNO reduction by measuring the endpoint NADPH concentration when either NADPH or GSNO was used as the limiting reagent. Similarly to the previously reported hFDH, CBR1 was seen to reduce GSNO with 1:1

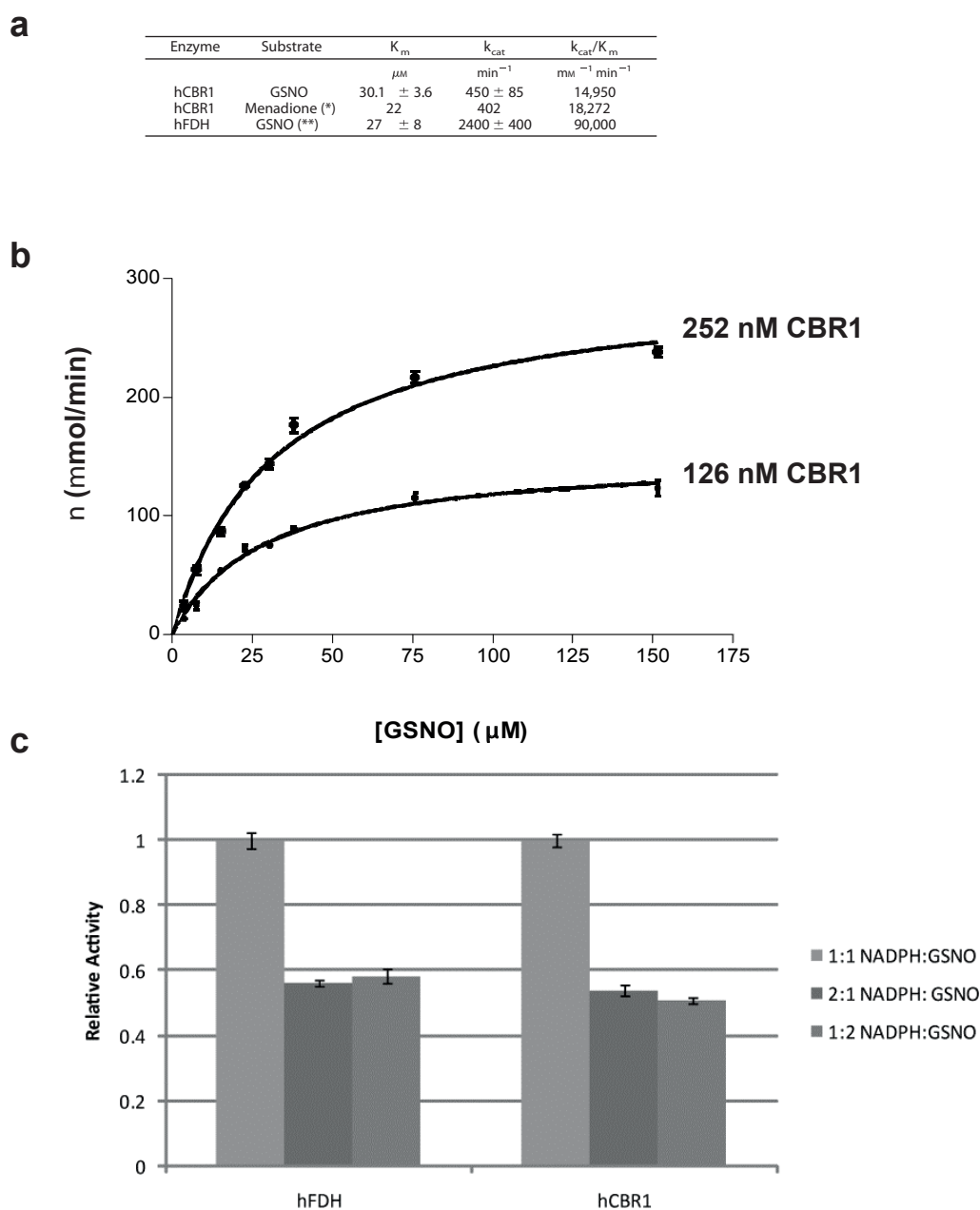


FIGURE 3. Kinetic data for CBR1 reduction. *a*, Comparison of kinetic constants for hCBR1- and hFDH-catalyzed GSNO reduction using NADPH and NADH, respectively; constants for CBR1 against menadione and FDH against GSNO were derived from *Tinguely, J. N., and Wermuth, B. (1999) Eur. J. Biochem. 260, 9–14 and **Hedberg, J. J., Griffiths, W. J., Nilsson, S. J., and Hoog, J. O. (2003) Eur. J. Biochem. 270, 1249–1256. *b*, Michaelis-Menten plot used to obtain kinetic constants for hCBR1 catalyzed GSNO reduction. *c*, hCBR1 and hFDH reaction stoichiometry. The extent of the reaction is decreased by approximately 50% when either the nicotinamide cofactor or GSNO is used as the limiting reagent.

stoichiometry with respect to NADPH. This suggested two possibilities for the transformation: 1) homolytic cleavage of the S-N bond to generate NO* and 2) 2-electron reduction of the N=O bond in a similar manner to a carbonyl. Possibility (1) would be expected to result in ultimate production of nitrite ion (through reaction of NO with dissolved oxygen), whereas possibility (2) would result in the ultimate production of either ammonia or hydroxylamine and deactivation of NO. hFDH has been demonstrated to function via the latter mechanism, so we measured endpoint concentrations of hydroxylamine, ammonia, and nitrite upon reduction of GSNO by either hFDH or hCBR1. In the absence of enzyme and chelating agent, GSNO was seen to produce significant amounts of nitrite, consistent with metal-catalyzed cleavage of GSNO and reaction with oxygen (similar to (1)). However, upon treatment with either hFDH or hCBR1 along with their corresponding cofactors, significant amounts of hydroxylamine and ammonia were produced, consistent with hydride donation to the –SNO nitrogen. Curiously, despite the fact that consumption of cofactor was verified spectrophotometrically, nitrite/hydroxylamine production is not stoichiometric under these conditions. Presumably, the unaccounted reaction balance is trapped in the form of glutathione sulfinamide (Figure 4); considering that these reactions are performed in the absence of free glutathione (which would tend to react with the N-(thio)hydroxylamine intermediate and trap reaction products as hydroxylamine and glutathione disulfide) and at a neutral pH (which would disfavor acidic hydrolysis of the sulfinamide to sulfinic acid and ammonia) it is not unreasonable to assume that the main product produced is the glutathione sulfinamide.

Cellular Reduction of GSNO by hCBR1

a

	NH ₂ OH	NH ₃	NO ₂ ⁻	Unaccounted
	μM	μM	μM	
hCBR1	30 ± 3	4.6 ± 0.4	<15	165
hFDH	23 ± 5	5.7 ± 0.4	<15	171
No enzyme ^a	14 ± 10	1.0 ± 1.0	31 ± 1	154

^a The background measurements were made in the absence of DTPA.

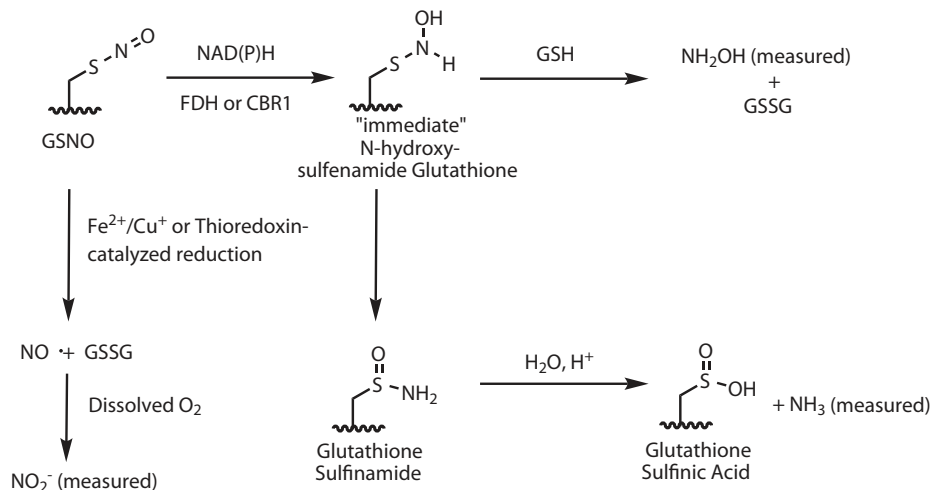
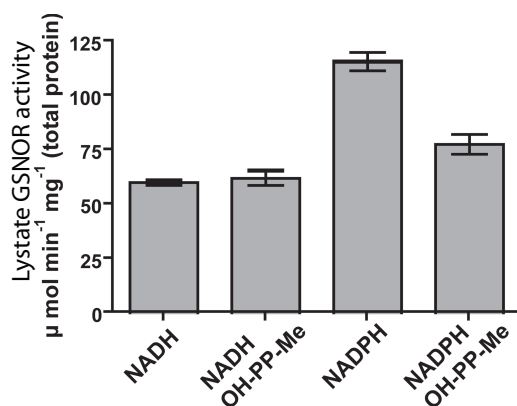
b**c**

FIGURE 4. In vitro analysis of GSNO reduction. a, quantitation of hydroxylamine/ammonia/nitrite for GSNO reduction by hCBR1, hFDH, or background processes in the presence of 200 mM GSNO and 200 mM NAD(P)H. b, proposed scheme for GSNO reduction by CBR1/FDH or background processes; enzymatic reduction is predicted to produce predominantly ammonia and sulfinic acid under limiting GSH. c, GSNO-reductase activity in A549 cell lysates in the presence of NAD(P)H with or without the selective hCBR1 inhibitor OH-PP-Me

Because hCBR1 was able to reduce GSNO with physiologically consistent kinetic constants in vitro, we next asked whether or not hCBR1 represented a significant amount of NADPH-dependent GSNO reductase activity in cells. We sought to measure the contribution of hCBR1 to GSNO-reductase activity of A549 cell lysates; however, this presented the problem of filtering out contributions of other GSNO reductases as well as nonenzymatic (i.e. metal/oxygen-catalyzed) reduction of GSNO. Because the other known GSNO-reductase is known to be NADH dependent, we measured GSNO reduction in the presence of NADPH or NADH; we also performed the reactions in the presence of iron/copper specific chelator (DTPA) to minimize nonenzymatic GSNO reduction. Further, because enzymes other than hCBR1 may contribute to NADPH-dependent GSNO reduction, we used treatment with a previously described specific inhibitor of CBR1 (OH-PP-Me¹⁴) to isolate the fraction of activity due to hCBR1. Consistent with the idea that GSNO reduction is mostly NADPH-dependent, GSNO reductase activity was seen to be higher in the presence of NADPH than NADH. Furthermore, NADPH reductase activity was decreased by ~30% upon treatment with OH-PP-Me, consistent with the idea that hCBR1 contributes to cellular reduction of GSNO.

Non-inhibitable NADPH-dependent GSNO Reductase Activity in Cells

A major question raised by this experiment was the origin of the residual GSNO reductase activity not inhibitable by OH-PP-Me in A549 cell lysates. While Liu et al.¹⁵ have implicated hFDH as the relevant NADH-dependent, GSNO-metabolizing enzyme in cellular lysate, no other NADPH-dependent GSNO metabolizing enzymes have been described in the literature. Two major possibilities are possible: 1) NADPH-dependent

activities that act on GSNO but do not cause its consumption and 2) an as-yet unidentified NADPH dependent GSNO reductase.

The obvious possibility for (1) is NADPH-dependent activity of thioredoxin, which has previously been demonstrated to generate free GSH and NO* by a hemolytic cleavage mechanism¹⁶. While this activity does not result in a net consumption of NO*, it nonetheless causes consumption of NADPH in a GSNO-dependent manner; due to the nature of the cellular assays used here (which follow oxidation of NADPH), this possibility cannot be eliminated as the origin of the OH-PP-Me resistant activity. It should be noted that the observed rate constant for this reaction (at least in the case of *E. coli* thioredoxin) is vastly lower (0.6 s^{-1}) than that of both hFDH (40 s^{-1}) and hCBR1 (7.5 s^{-1}) for GSNO; however, the relatively high reported concentration of reduced thioredoxin in cells ($2\text{-}14 \mu\text{M}$ ¹⁷) make thioredoxin a likely candidate for the residual NADPH dependent activity.

The obvious possibility for (2) is the poorly characterized SDR family member hCBR3, which exhibits 72% identity with hCBR1 and also appears to be an NADPH-dependent quinone reductase¹⁸. A crystal structure for hCBR3-NADP+ (pdb code 2HRB¹⁹) has recently been reported in the literature, so we generated a structural alignment with hCBR3-NADP+-OH-PP-GSH (pdb code 3BHJ) to determine if hCBR3 might also bind glutathione and/or be inhibited by pyrrolopyrimidines. Immediately obvious in the structural comparison is the absence in hCBR3 of what appears to be a critical packing residue (W229) forming the bottom of the OH-PP binding pocket and substitution of M141 (which appears to form the “top” of the binding pocket) for glutamine (Q142) creating a larger and less hydrophobic binding site. This would seem to suggest that OH-PP would not be active against hCBR3 in cell lysate. Comparison of the glutathione binding region finds substitution of multiple residues in hCBR3 (A192P,

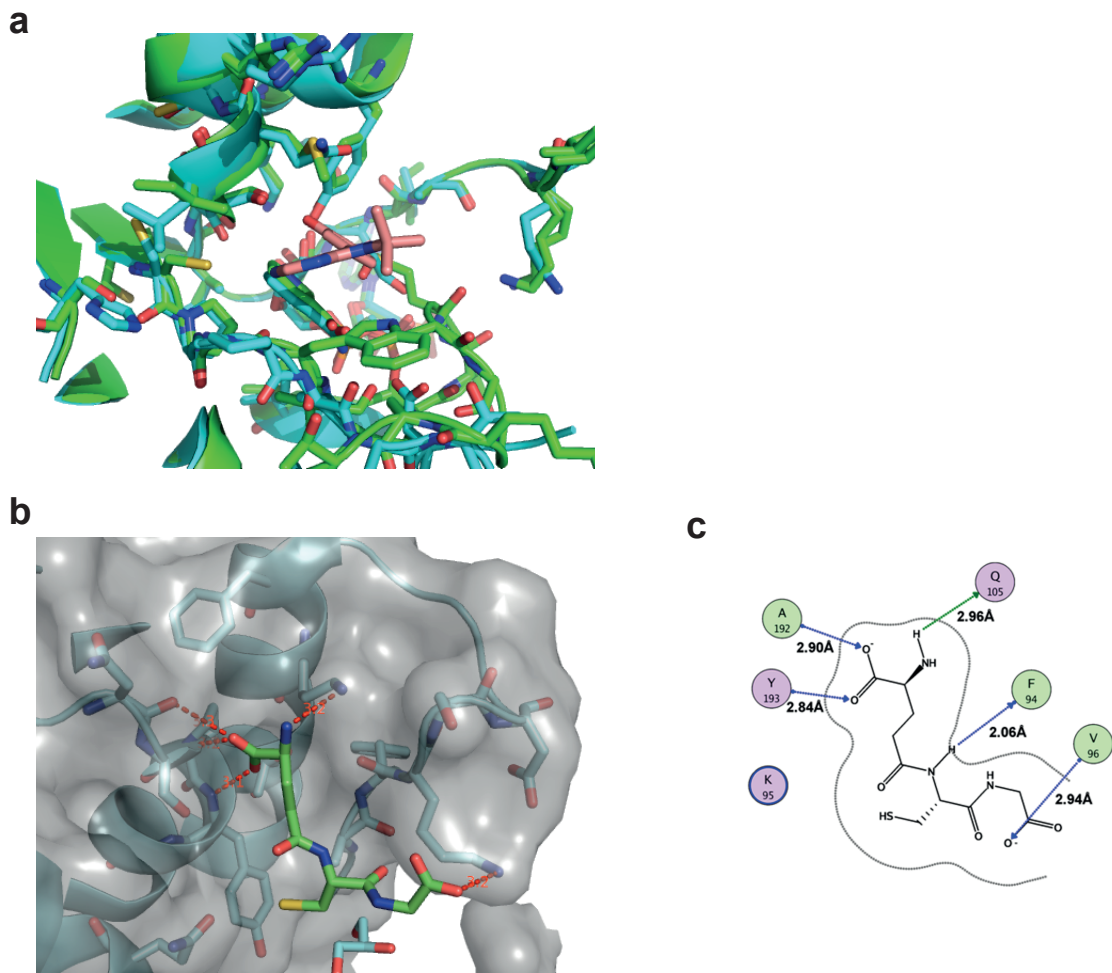


FIGURE 5. Structural comparison of hCBR1 (pdb 3BHJ) and hCBR3 (pdb 2HRB). a, comparison of OH-PP binding to CBR1 (green) and CBR3 (cyan); CBR3 lacks critical W220 residue and has an M141->Q142 structural substitution which combined may oblate OH-PP binding. b, putative glutathione binding to CBR3; glutathione is capable of forming similar main-chain hydrogen bonds with CBR3 residues. c, schematic of glutathione binding to CBR1.

Q105K, V96S) that are involved in polar contacts with glutathione in hCBR1; nonetheless the glutathione binding site does not seem to be occluded in hCBR3 and an analogous (but not identical) series of polar contacts can be proposed for interaction of glutathione with hCBR3. Thus, in the absence of enzymatic data for GSNO reduction, the possibility of hCBR3 as a contributor to the OH-PP resistant reductase activity in cell lysates must be considered.

Significance of CBR1 as a GSNO Reductase—Detoxification of Nitrosothiol Excess?

The putative role of CBR1 as an S-nitrosoglutathione reductase in cells would initially seem to be in conflict with previous data implicating a role for CBR1 as a general protectant against cellular chemical stressors. The wide substrate selectivity of CBR1 for an SDR-family reductase and its elevation in tissues such as brain and liver that are subject to oxidative/toxic insults would suggest CBR1 counteracts various chemical insults. In contrast, S-nitrosylthiols have been shown to function in cytoprotective processes such as caspase inhibition and sGC/protein kinase G activation—and CBR1 activity against GSNO would be expected to counteract these processes. While it is entirely likely that CBR1 activity could be relevant for different reasons in different locations, the simplest way to resolve this apparent paradox would be to simply note that while S-nitrosylation has been shown to have a cytoprotective role, it is abundantly clear that *excessive* S-nitrosylation is an apoptosis-inducing stress; apoptosis can be induced upon treatment with either NO-donors such as GSNO or by cytokines that activate NO production by iNOS²⁰. It is not difficult to conceive of situations that may produce similar nitrosative insults to treatment with chemical NO-donors; uncontrolled immune responses resulting in excessive NO production by microglia or immune cells is one

such example. In this context, GSNO reductases like CBR1 could be seen as a last line of defense against excessive S-nitrosothiol levels or overly long durability of NO signaling. In this sense, the function of CBR1 would seem to be consistent with its previously delineated roles in xenobiotic detoxification and reactive species neutralization—that is, to protect normal cells from toxicity of nitrosothiol excess.

Experimental Methods

K_m Determination for the Substrate GSNO—Human carbonyl reductase 1 activity was determined spectrophotometrically as previously described¹⁴. The reactions contained 100 μM NADPH in 50 mM sodium phosphate (pH 6.8) and either 252 nM or 126 nM hCBR1. GSNO substrate was prepared by combining stoichiometric amounts (0.5 M each) of GSH, sodium nitrite, and HCl. Diethylenetriaminepentaacetic acid (1 mM) was added to prevent decomposition because of metal ion contamination. The yield of GSNO was verified spectrophotometrically by measuring the absorption of the created SNO group at 335 nm using an extinction coefficient of 0.92 mM⁻¹ cm⁻¹. The aqueous GSNO solution was added to samples to achieve concentrations of 151.4, 75.7, 37.85, 30.3, 22.7, and 15.1 μM. All of the reactions were performed in triplicate. The initial rates were calculated from the absorbance decrease (340 nm) using a combined extinction coefficient of 7.06 mM⁻¹ cm⁻¹ for GSNO and NADPH and were applied to the Marquardt-Levenberg algorithm for *K_m* determination. The *k_{cat}* was determined at saturating

substrate concentration (200 μ M NADPH and 200 μ M GSNO) using hCBR1 that had been purified by size exclusion chromatography¹⁴ and never frozen.

Determination of NADPH and GSNO Stoichiometry—Reactions were prepared in 50 mM sodium phosphate with 126 nM recombinant hCBR1 including 100 μ M NADPH and 50 μ M GSNO, 50 μ M NADPH and 100 μ M GSNO, or 50 μ M NADPH and 50 μ M GSNO. Stock solutions of GSNO contained diethylenetriaminepentaacetic acid (1 mM), and the concentration was verified spectrophotometrically at 335 nM. The reactions were performed in triplicate, and the combined decrease in NAD(P)H and GSNO absorbance was determined at the end point for each reaction. Additionally, reaction stoichiometry was determined for human glutathione-dependent formaldehyde dehydrogenase (hFDH) in an analogous manner using NADH.

Determination of Nitrite, Hydroxylamine, and Ammonia—The samples (1 ml) were prepared containing 250 mM sodium phosphate, 200 μ M GSNO (prepared as above), and 200 μ M of either NADH or NADPH. The reactions were initiated by the addition of FDH or hCBR1 respectively and allowed to continue for 1 h at 25 °C. Absorbance was monitored at 340 nm to verify that the reactions were complete. The samples were maintained at -80 °C until analyzed.

For all of the determinations, the standards were prepared in the assay buffer (250 mM sodium phosphate (pH 6.8). Nitrite concentration was determined by use of the modified Greiss reagent (Sigma) using the manufacturer's protocol. Hydroxylamine concentration was determined in a manner similar to the procedure of Jensen et al. (Jensen, D. E., Belka, G. K., and Du Bois, G. C. (1998) *Biochem. J.* 331 659-668).

Briefly, 300 μ l of 100 mM sodium phosphate (pH 4.4) was added to 100- μ l sample. Then 200 μ l of 1% (v/v) 8-hydroxyquinoline in 50% aqueous ethanol was added with mixing and followed by 200 μ l of 1 M sodium carbonate. The samples were heated to 95 °C for 7 min and cooled on ice for 1 h, and the absorbance (750 nm) was determined. The hydroxylamine concentration was determined by comparing the sample absorbances to a standard curve prepared with samples containing hydroxylamine-HCl. Ammonia concentration was determined following instructions in the Sigma ammonia diagnostic kit. The standards were prepared using ammonium sulfate in assay buffer.

GSNO Reductase Activity from A549 Cell Lysates—A549 cells were cultured using F-12K medium containing 10% fetal bovine serum, penicillin, and streptomycin. Following removal of medium, the cells were washed twice with 1 \times phosphate-buffered saline and incubated with lysis buffer (150 mM NaCl, 1% Nonidet P-40, 50 mM Tris-Cl, 1 mM dithiothreitol, pH 8.0) at 4 °C for 20 min. The lysates were subsequently clarified by centrifugation (14,000 \times g, 10 min), and the protein concentration was determined using the Bio-Rad DC protein assay. The activities were determined spectrophotometrically as above by subtracting the background rate of NADPH/GSNO reduction in the absence of lysate. The reactions were performed in triplicate using 1-cm-path length cuvettes containing 100 μ M NADPH or NADH with and without the addition of 100 μ M OH-PP-Me. Sodium phosphate (50 mM, pH 6.8) and GSNO (100 μ M) were present in all reactions.

References

1. Kavanagh, K.L. et al. Medium- and short-chain dehydrogenase/reductase gene and protein families : the SDR superfamily: functional and structural diversity within a family of metabolic and regulatory enzymes. *Cellular and molecular life sciences : CMLS* **65**, 3895-906(2008).
2. Wrighton, S. a & Stevens, J.C. The human hepatic cytochromes P450 involved in drug metabolism. *Critical reviews in toxicology* **22**, 1-21(1992).
3. Tomlinson, J.W. et al. 11Beta-Hydroxysteroid Dehydrogenase Type 1: a Tissue-Specific Regulator of Glucocorticoid Response. *Endocrine reviews* **25**, 831-66(2004).
4. Wermuth, B. et al. Carbonyl reductase provides the enzymatic basis of quinone detoxication in man. *Biochemical pharmacology* **35**, 1277-82(1986).
5. Doorn, J. a et al. Human carbonyl reductase catalyzes reduction of 4-oxonon-2-enal. *Biochemistry* **43**, 13106-14(2004).
6. Bains, O.S. et al. Two nonsynonymous single nucleotide polymorphisms of human carbonyl reductase 1 demonstrate reduced in vitro metabolism of daunorubicin and doxorubicin. *Drug metabolism and disposition: the biological fate of chemicals* **37**, 1107-14(2009).
7. Holleran, J.L. et al. In vitro metabolism of the phosphatidylinositol 3-kinase inhibitor, wortmannin, by carbonyl reductase. *Drug metabolism and disposition: the biological fate of chemicals* **32**, 490-6(2004).

8. Wirth, H. & Wermuth, B. Immunohistochemical localization of carbonyl reductase in human tissues. *The journal of histochemistry and cytochemistry : official journal of the Histochemistry Society* **40**, 1857-63(1992).
9. Chung, H., Fried, J. & Jarabak, J. Irreversible inhibition of the human placental NADP-linked 15-hydroxyprostaglandin dehydrogenase/9-ketoprostaglandin reductase by glutathione thiosulfonate. *Prostaglandins* **33**, 391-402(1987).
10. Gaston, B. et al. S-nitrosothiol signaling in respiratory biology. *American journal of respiratory and critical care medicine* **173**, 1186-93(2006).
11. Tinguely, J.N. & Wermuth, B. Identification of the reactive cysteine residue (Cys227) in human carbonyl reductase. *European journal of biochemistry / FEBS* **260**, 9-14(1999).
12. Williamson, D.H., Lund, P. & Krebs, H.A. The redox state of free nicotinamide-adenine dinucleotide in the cytoplasm and mitochondria of rat liver. *The Biochemical journal* **103**, 514-27(1967).
13. Veech, R.L., Eggleston, L.V. & Krebs, H.A. The redox state of free nicotinamide-adenine dinucleotide phosphate in the cytoplasm of rat liver. *The Biochemical journal* **115**, 609-19(1969).
14. Tanaka, M. et al. An unbiased cell morphology-based screen for new, biologically active small molecules. *PLoS biology* **3**, e128(2005).
15. Liu, L. et al. A metabolic enzyme for S-nitrosothiol conserved from bacteria to humans. *Nature* **410**, 490-4(2001).

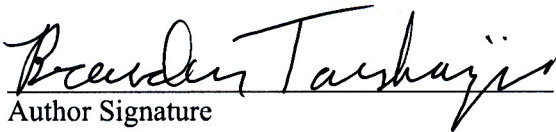
16. Nikitovic, D. & Holmgren, a S-nitrosoglutathione is cleaved by the thioredoxin system with liberation of glutathione and redox regulating nitric oxide. *The Journal of biological chemistry* **271**, 19180-5(1996).
17. FERNANDO, M.R. et al. Thioredoxin regenerates proteins inactivated by oxidative stress in endothelial cells. *European Journal of Biochemistry* **209**, 917–922(1992).
18. Miura, T., Nishinaka, T. & Terada, T. Different functions between human monomeric carbonyl reductase 3 and carbonyl reductase 1. *Molecular and cellular biochemistry* **315**, 113-21(2008).
19. Pilka, E.S. et al. Structural basis for substrate specificity in human monomeric carbonyl reductases. *PloS one* **4**, e71113(2009).
20. Eu, J.P. et al. An apoptotic model for nitrosative stress. *Biochemistry* **39**, 1040-7(2000).

Publishing Agreement

It is the policy of the University to encourage the distribution of all theses, dissertations, and manuscripts. Copies of all UCSF theses, dissertations, and manuscripts will be routed to the library via the Graduate Division. The library will make all theses, dissertations, and manuscripts accessible to the public and will preserve these to the best of their abilities, in perpetuity.

Please sign the following statement:

I hereby grant permission to the Graduate Division of the University of California, San Francisco to release copies of my thesis, dissertation, or manuscript to the Campus Library to provide access and preservation, in whole or in part, in perpetuity.


Author Signature

1/10/11
Date